Response to referee comment #1

This study presents a comprehensive evaluation of the CRE of low-level Arctic clouds in ICON simulations above sea-ice covered surfaces. Low-level clouds and in particular mixed-phase clouds impact the surface radiative balance substantially in this region and are often miss-represented in climate models. This analysis is thus addressing one of the key concerns within the community and will be of interest to a wide readership. The paper is really well written and very logically structured. Their results are presented clearly and concisely and I agree with their scientific conclusions. Occasionally their arguments could be strengthened, which I point out in my comments below. Overall, I think this is an excellent paper that deserves publication once these minor revisions are addressed.

We thank the reviewer for the constructive comments that helped to improve the manuscript.

General comments

1. I understand that the case descriptions etc. are given in other papers. Yet from this paper it isnot clear for which conditions you have tested the TKE-based activation approach and its impact on net CRE and for which conditions you associate the largest biases. While detailed case descriptions are not necessary, context should be given for the reader in terms of the conditions of June 2nd-June 5th (for which the bias attribution and sensitivity analysis is done). In particular information with respect to temperature regime, integrated water vapour content, optical depth regime, precipitation characteristics and stability would be useful. Also are these predominantly stratiform or broken cloud-decks? I would also suggest to contextualise your findings in the discussion section in terms of how far you would be comfortable to extrapolate your findings beyond the optically thin (I assume), single-layer cloud regime that you explored here in greater detail.

A more elaborate description of the prevailing conditions during the period of interest is now given in the revised manuscript. This includes a quantification of the temperature and humidity regime. Additional information is given on the state of the atmospheric boundary layer, as well as on the cloud regime that prevailed during that period.

Regarding the question whether our findings can be extrapolated to conditions beyond the cloud regime on which we focused on in this study (i.e. optically thin single-layer clouds), we additionally analyzed days with multi-layer clouds being present, which was the case in mid June 2017. We find a similar overestimated transmissivity and stronger warming effect of clouds in ICON compared to the observations. This information has been added to the conclusions in the revised manuscript.

2. You argue the utility and necessity to evaluate and improve kilometre-scale simulations. In this paper you provide a pathway to improve the simulated net CRE for "kilometre-scale" ICON simulations for Arctic low-level clouds, which may even yield to improvements to similar cloud regimes simulated in other regions of the globe. In order to use this approach more widely, it would be helpful to be aware of its potential limitations within the range of "kilometre-scale" grids. Here, you show results of a particular configuration of horizontal (1.2km resolution) and vertical resolution. Terms like "kilometre-scale", "convection-permitting", etc. are often used in the community for a range of resolutions ranging from, say, 1-5 km, which apply all kinds of vertical grid refinement within the boundary layer. How valid do you expect your conclusions to remain across the range of spatial resolutions that fall under the category "kilometre-scale"/"convection-permitting"? Would you expect your TKE fix to droplet activation to work equally well at a (say) 5km grid spacing, or when only half the vertical grid spacing is applied?

To quantify whether our pathway to improve cloud microphysics in Arctic clouds can also be employed at higher spatial resolution in the horizontal and in the vertical, we did two sensitivity studies. As simulations at 5 km would have implied a substantial effort due to the fact that we would have to completely redo the generation of the input data (i.e. grid, external parameters and forcing data), we only looked at the effects on the outer domain of our set-up, which has a horizontal resolution of 2.4 km. Additionally, we did another simulation at 2.5 km in which we reduced the number of vertical levels from 75 to 50, which is comparable to the vertical resolution of present-day climate models.

The histograms of hydrometeor diameter, number concentration and liquid water content at 2.4 km resolution with 75 vertical levels (Figure 1) and at 2.4 km resolution with 50 vertical levels (Figure 2) are almost identical to the Fig. 6 in the revised manuscript at 1.2 km. Still, 2.5 km is still on the finer end of kilometer-scale simulation.
In our set-up, TKE is used to include subgrid-scale vertical motion in the activation of CCN into cloud droplets. A similar parameterization for the activation of CCN due to subgrid-scale vertical motion has been used at even coarser resolutions of 20 km (Morrison and Pinto, 2005). Nevertheless, in such an activation parameterization, it is crucial that grid-scale TKE is correctly parameterized. In ICON, this quantity is calculated from a prognostic TKE scheme following Raschendorfer (2001). As this TKE scheme is also used for the operational ICON performed at global scale with a resolution of more than 10 km makes us confident that it should also perform reasonably well at resolution larger than 2.4 km. Therefore, we are confident that this activation parameterization can be employed for coarser resolution in ICON and also for kilometer scale simulation in models that employ a two-moment scheme. A summary of these new results has been added to the revised manuscript

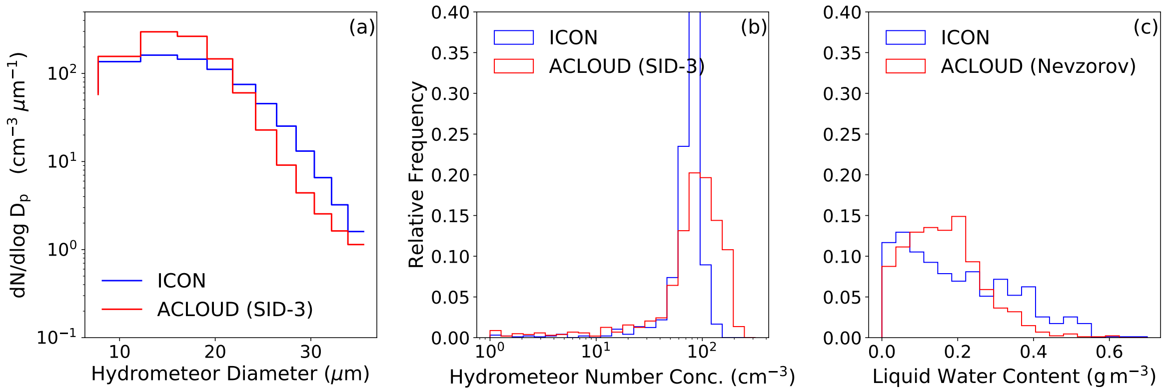

Figure 1: As Fig. 6 in the revised manuscript but at a horizontal resolution of 2.4 km and with 75 vertical levels.

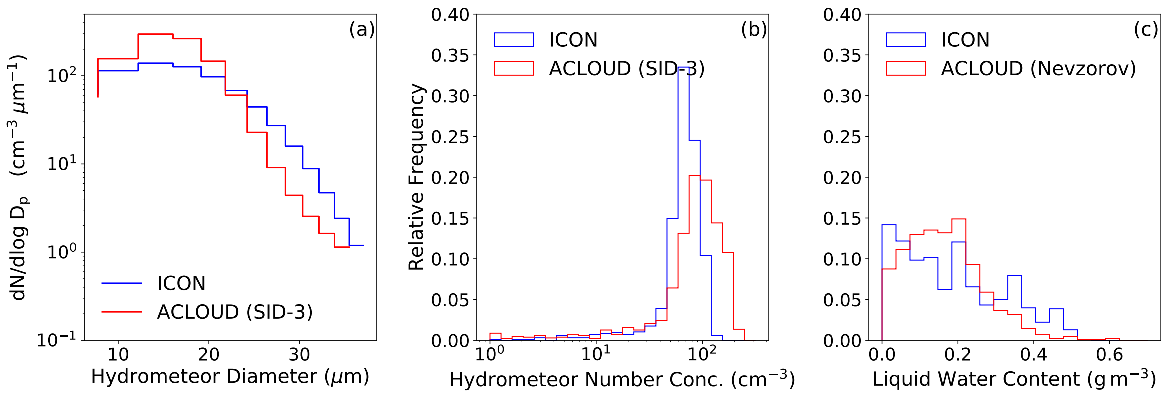

Figure 2: As Fig. 6 in the revised manuscript but at a horizontal resolution of 2.4 km and with 50 vertical levels.

3. In section 3 during your evaluation of surface radiative quantities you argue that you can compensate for the temporal irregularity of your model output (every 3h) by the increased spatial coverage and thus increased sampling of spatial variability. This essentially assumes that spatial and temporal variability are equivalent. This is assumption is commonly made during simulation-observation comparisons. Can you demonstrate this to be valid though forradiative quantities subject to a diurnal cycle?
The output frequency of our model simulations is 30 minutes (3 hours is the frequency of the forcing

data from the IFS). This implies that the largest temporal difference between an observational data point and the output timestep of ICON is ± 15 minutes. To illustrate the effect of this temporal inconsistency, we plotted the bias in incoming solar radiation at TOA introduced by the limited model output frequency and the applied temporal sampling (Figure 3). The bias is largest ($\pm 14\,\mathrm{W\,m^{-2}}$) at 7 and 19 UTC when the temporal derivative of incoming solar radiation is the largest. During noon when most of the research flights took place, this bias is substantially smaller. Considering that we focused our analysis mainly on cloudy conditions, this maximum bias is further reduced and probably on the order of a few $\mathrm{W\,m^{-2}}$. Additionally, if long enough periods are considered, any bias will eventually average out. Especially for the period of the sensitivity study where only a limited amount of low-level section are available, this can not be fully ensured. Nevertheless, we are confident that this issue will not significantly influence the overall findings in this study as the biases found are almost one order of magnitude larger than the biases introduced by the limited model output frequency. We summarize this result in the revised manuscript.

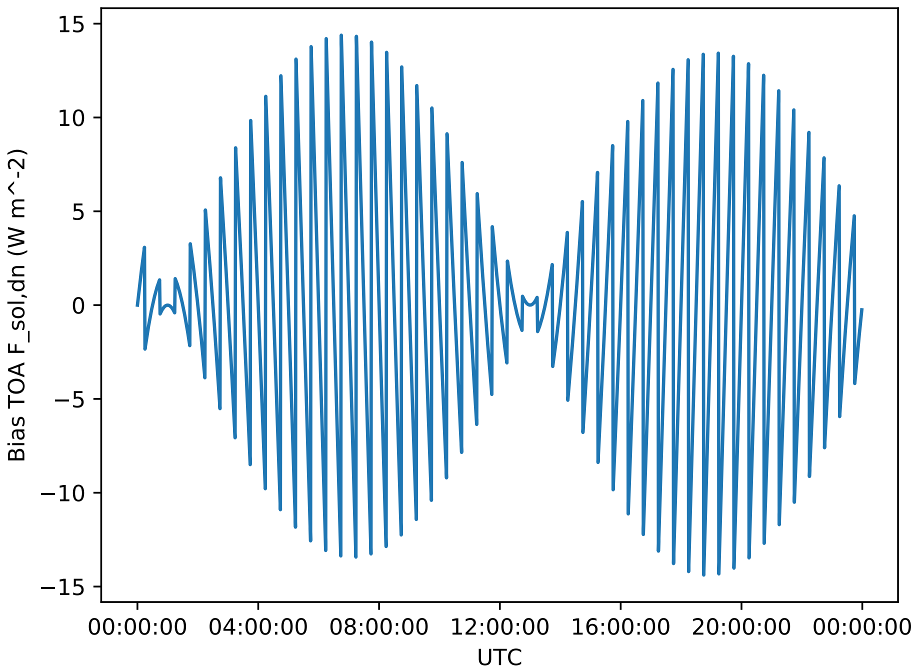

Figure 3: Bias in incoming solar radiation at TOA at 80° N for 1 June introduced by the limited model output frequency and applied temporal sampling.

4. Your analysis of biases regarding net CRE is focused on the period of 2-5th of June. In L234 you state that you select this period because you largely are dealing with single-layered low-level clouds and have a high density of flights. I am assuming that the bias in CRE (Fig. 4) is also largest during this time period and for this particular cloud regime as well? Given the significance of the analysis that follows for the overall manuscript, I would include a couple more sentences on this selection for clarity.

Those days were mainly selected due to similar meteorological conditions that enabled a statistical aggregation of those days. Furthermore, in-situ observations of microphysical properties were performed on all flight days. The day with the largest bias in CRE has been observed on 14 June, but this was a day with a lot of multi-layer clouds present, which made the interpretation of the bias in CRE much harder than for single layer clouds. In the revised manuscript, we give more information of why this period was chosen and also to which extent the bias in CRE can be observed for other meteorological conditions (see also reply to general comment #1).

5. I agree with your general sentiment conveyed in the introduction and conclusion sections of this manuscript that high-resolution LES simulations are quite limited in their spatial and temporal coverage and that coarser-resolution simulations allow longer-term evaluations over larger domains. Yet I wonder, if you are not subject to the same limitations in this particular application, since you are restricting this evaluation to the location of 15 linear flight tracks within a particular region (although admittedly you can afford to simulate more flight hours), and most of your analysis is focused on the period June 2nd-5th. The argumentation of the benefits and limitations of kilometre-scale versus LES simulations does not seem an essential part of your analysis. Thus I would consider to reduce the emphasis on this point, as this is not something you actually show.

Indeed, for the limited domain where research flights took place, the larger spatial coverage of simulations at kilometer-scale might not be needed. Nevertheless, the ability of being able to afford a large amount of sensitivity studies would be extremely resource intensive at finer resolution and, therefore, simulations at kilometer-scale are a good compromise. As proposed by the reviewer, we shortened the pros-and-cons discussion of kilometer-scale versus LES simulations in the revised manuscript.

6. Fig. 6 very clearly shows the bias in simulated cloud properties that are consistent with an overestimation in cloud transmissivity. From the observations you are under constrained and cannot (I presume) say with certainty whether this is a source or sink issue. In your analysis you show that the bias can be fixed by increasing the source in Nd. Can you provide an equally strong argument, that you could not obtain the same improvement, by adjusting the sink? I think this could be done in the context of a discussion of cloud-base or surface precipitation rates, or a couple of additional numerical experiments where you explicitly show that adjustments to the autoconversion rate by: either turning it off altogether – essentially shutting off warm rain – or reducing its efficiency, does not yield the same kind of improvement.

We performed an additional sensitivity study in which autoconversion was turned off completely. While the effect on liquid water content is comparable to the revised, but not yet scaled CCN activation (see Fig. 7), the cloud droplet number concentration is still slightly underestimated. Furthermore, the shape of particle number size distribution still does not really match the shape of the observed size distribution. Since the CCN profile used in the activation of CCN into cloud droplets within the cloud microphysical scheme is not suited for an Arctic domain as it overestimates the availability of CCN, the underestimated amount of cloud droplets in the simulations with autoconversion turned off is a further indication that it is rather a source than a sink problem. We furthermore looked at CRE for turned off autoconversion (not shown). The effect of turning off autoconversion altogether is comparable to the effect of revised CCN activation (see Fig. 9b), as the CDNC used in the radiation routine is a constant profile and not coupled to the cloud microphysics. As the source-or-sink discussion is an important aspect, we added this discussion to the revised manuscript.

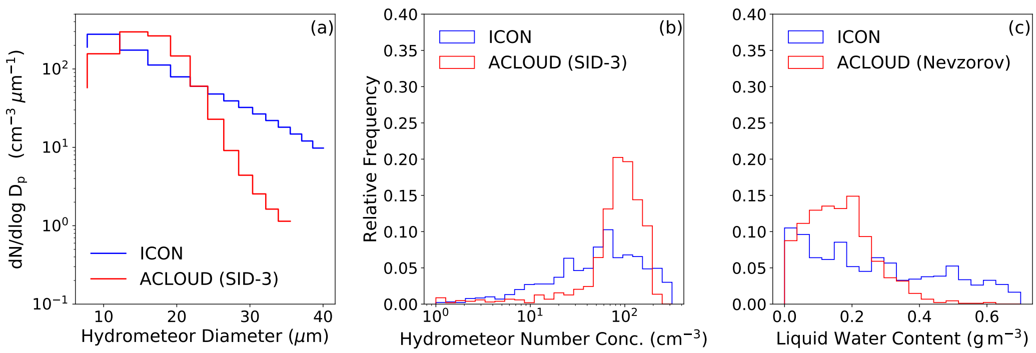

Figure 4: As Figure 6 in the revised manuscript, but with autoconversion turned off.

General comments

1. L44: This seems like a somewhat random selection of LES studies in the Arctic and by no means complete. I suggest to either include a comprehensive list of references, or to make it clear that this list of studies is merely exemplary.
An "e.g." has been added to clarify that this list of studies is merely exemplary.

2. L48ff: In addition to the representation of in-cloud turbulence and cloud-top inhomogeneity, LES setup also allows the study and evaluation of microphysical processes (e.g. Ovchinikov et al. (2014), Solomon et al. (2015), Fridlind et al. (2017)) and aerosol-cloud interactions (e.g. Possner et al. (2017), Solomon et al. (2018), Eirund et al. (2019)) at scales where the dynamics and thermodynamics are largely resolved. Since you identify the representation of CCN and the activation process itself as one of your primary sources of bias regarding net CRE. It seems fair to mention this here.
Refs:
1.Ovchinikov et al (2014): doi:10.1002/2013MS000282 (JAMES)
2.Fridlind et al (2017): doi:10.1029/2007JD008646 (JGR)
3.Solomon et al (2015): doi:10.5194/acp-15-10631-2015 (ACP)
4.Possner et al (2017): doi:10.1002/2016GL071358 (GRL)
5.Solomon et al (2018): https://doi.org/10.5194/acp-2018-714 (ACP)
6.Eirund et al (2019): https://doi.org/10.5194/acp-19-9847-2019 (ACP)

Thank you for pointing us to these references. We added a sentence that highlights the use of LES with regards to the evaluation of cloud microphysical processes and aerosol-cloud interactions in the Arctic.

3. L102: What is your reasoning for using the all or nothing cloud-cover scheme? Did it impact your results?
The all-or-nothing cloud cover scheme was mainly chosen to facilitate the comparison of the simulations with the observations. Having fractional cloud cover in the simulation would imply the need to divide microphysical properties by the fractional cloud cover to get the respective in-cloud values, that are present in the observational dataset. For that reason, we decided to use an all-or-nothing cloud cover scheme where this is not necessary. At the resolutions used in this study, an all-or-nothing cloud cover scheme might miss some clouds as the necessary saturation humidity might not be reached, which might be especially problematic for weak dynamical forcing. The cloud fields and also the radiative properties of clouds between the all-or-nothing cloud cover scheme and a cloud cover scheme that allows for fractional cloud cover were relatively similar along the flight track of the research flights, which made us confident that resolving clouds at grid scale only is sufficient for our set-up.

4. L132: "The daily averaged observed albedo is parameterized as a function of day of the year". I did not follow this. Did you not simply prescribe the daily mean albedo value from the full sea-ice covered surface observations. So how is it a "function" of the day of year?
Due to the fact that the campaigns took place at the onset of the melting period, the sea ice albedo significantly reduced in that timespan. To this end, we prescribed the sea ice albedo derived from aircraft observations over fully sea ice covered regions to be consistent with that evolution and, therefore, have parameterized the sea ice albedo as a function of time (i.e. day of the year). The description of this approach has been revised to be better understandable.

5. L177/178: Why did you not fix the sea ice fraction in a similar fashion as the sea ice albedo in your simulation setup to exclude the impact of biases from essentially prescribed surface properties?
We opted against prescribing sea ice fraction because one would only be able to prescribe sea ice fraction along the flight track as a generalized formulation would not be possible due to the highly spatially variable nature of sea ice fraction. Such a spot change would not significantly affect the thermodynamic profile in a dynamic clouds field and, therefore, not affect the resulting consequences on cloud macro- and microphysical properties. For that reason, only the differences in surface albedo

will affect the radiative effect of clouds along the flight track, which we qualitatively discuss in the manuscript.

6. L217: I agree with your conclusion that the underestimated cooling in the solar spectral range is likely due to an incorrect simulation of cloud transmissivity, rather than remaining biases in surface albedo. As this a central aspect to your overall argument, I was wondering if you could not show this explicitly. Do your conclusions remain the same if you restrict the phase space your analysis of the observations to surface albedo values < 0.8 *such as to match the simulations?*
Constraining the phase space of the observations by imposing an upper limit for the allowed surface albedo values is indeed a good idea. Instead of the proposed threshold of 0.8, we decided to choose an upper bound of 0.85, which is equivalent to the daily averaged maximum albedo value used in our adapted albedo parameterization. This threshold has now been applied to all plots in the revised manuscript. The effect of this upper albedo threshold can mainly be seen in changes of the radiative properties in the ACLOUD data due to the reduced surface reflectivity. Due to the fact that the respective datapoints in both datasets have to fulfill the chosen condition at the same time, also small changes can be observed for the ICON data. Nevertheless, the general conclusions using an upper threshold for the surface albedo stay the same.

7. L231: I personally would argue that cloud water content is to first order a thermodynamic variable and thus also a macrophysical variable that is adjusted by microphysical processes (i.e. the efficiency of autoconversion/accretion in warm-phase clouds anyway). Especially in a model with saturation adjustment I have a hard time referring to qc as purely microphysical, but can be convinced.
It is correct that cloud water content should not solely be considered as a microphysical variable. We clarified that in the revised manuscript.

8. "it shows a slight underestimation". Can you quantify this? What is the average/median cloud depth?
The mean cloud depth bias of the model compared to the observation is 65 m. This quantification has been added to the revised manuscript.

9. L260: I would suggest to be more specific/quantitative here, as this is a key argument in your assertion that the bias stems predominantly from biases in cloud water content and droplet concentration. For the typical cloud optical depth seen in your simulations or during the observation record, how large would a geometrical cloud depth bias have to be to affect transmissivity substantially? How does that quantity relate to your biases assessed? In that context, I am not sure Fig. 5 is best suited. I wonder if a PDF-based comparison is not more informative. Cloud transmissivity is strongly non-linearly related to geometrical cloud depth. Thus biases in the distribution of geometrical depth (although means may agree), could induce substantial biases in mean cloud transmissivity. To follow your line of assertion, the argument that cloud depth biases are unlikely to contribute signficantly should be strengthened quantitatively.
To explore the effect of a larger geometrical cloud depth on the CRE, we used in-situ profiles of LWC from 4 June that have been observed close to R/V Polarstern and linearly interpolated the LWC with altitude (Figure 5). To calculate the CRE, we used offline radiative transfer simulations (for more details on those simulations, see section 3.2 in the revised manuscript). The albedo used in these simulations is set 0.835, which is the mean albedo value for that day. From the profile of LWC and temperature, we estimate the geometrical cloud depth to be around 290 m for that day, which is in accordance with what has been observed from R/V Polarstern. Looking at the change of $\mathrm{CRE_{sol}}$ with vertical cloud extend, we find an almost linear relationship between the two quantities. If one would reduce the vertical cloud extend by 65 m, the $\mathrm{CRE_{sol}}$ would approximately increase by $5\,\mathrm{W\,m^{-2}}$. We repeated the estimation of the bias introduced by the non-matching vertical cloud extend for other vertical profiles that had lower adiabaticity factors than in this case and the obtained biases in $\mathrm{CRE_{sol}}$ were in a similar range. As the bias in $\mathrm{CRE_{sol}}$ between ICON and the observations for the days of the sensitivity studies is more than $20\,\mathrm{W\,m^{-2}}$, we are confident that the bulk of this bias is actually

caused by misrepresented cloud microphysical properties in ICON. The deviations to the solar CRE observed by ACLOUD for the period from 2 June to 5 June (see supplement) can be explained by the higher albedo used in the offline radiative transfer simulations compared to the flight sections used there. This is now reported in the revised manuscript.

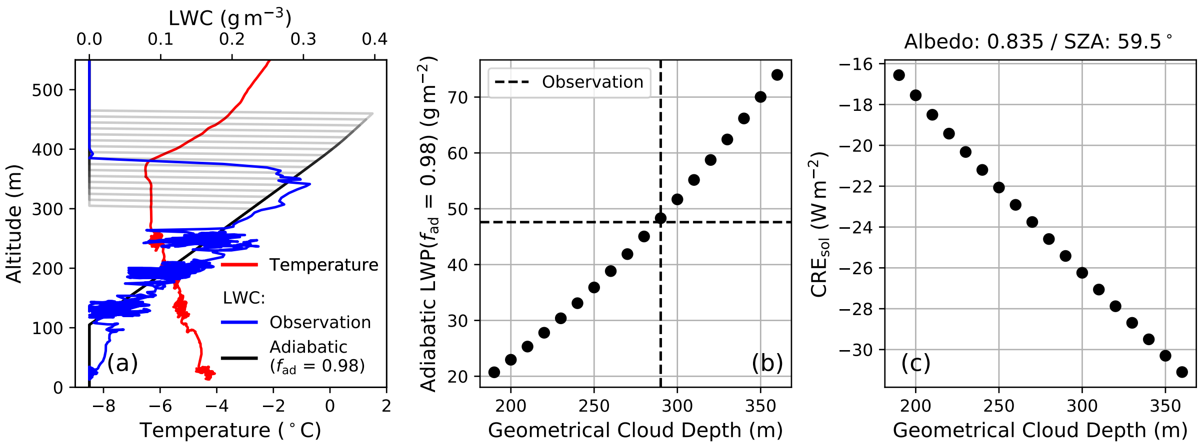

Figure 5: (a) Observed in-situ vertical profile of temperature (red) and liquid water content (blue) for vertical profile near R/V Polarstern on 4 June. The black line is the linearly interpolated LWC with an adiabaticity factor f_{ad} of 0.98.(b) LWP as a function of geometrical cloud depth using with f_{ad} of 0.98. The dashed lines indicate the observed geometrical cloud depth and LWP. (c) CRE_{sol} as a function of geometrical cloud depth. CRE_{sol} has been derived from offline radiative transfer simulations using the respective LWP as calculated in (b). Deviation of CRE_{sol} compared to what has been observed by ACLOUD (see Fig. S3 in the supplement) stem from lower albedo ($\sim$ 0.79) in these flight sections compared to the offline radiative transfer simulations (0.835).

10. L270: "droplets plus ice crystals": essentially droplet concentration at $<1\,cm^{-3}$. I would not expect to see any impact of ice in the shown range. It may be worth to state explicitly.
Done.

11. L300: Can you provide a quantitative estimate of rain rate? Do you have any constraint here from the observation?
We added a quantitative estimate of modeled rain- and snow rate in the region around R/V Polarstern to the revised manuscript. Unfortunately, no observations of surface precipitation was available.

12. Fig 2: In the range of surface albedos between 0.6-0.8 where the number of occurrence is highest, the simulations show a much considerably narrower range of $F_{net,sol}$ than the observations. Do you have any idea whether this is indicative of a model bias, or simply a sampling issue between the simulation and observation datasets?
As stated in the manuscript, low albedo values are related to days towards the end of the campaign when cloud free conditions were present. Such a day was the 25 June, that a had a relatively large amount of low-level sections. In contrast to the observations, clouds were present in the model on that day, causing a negative bias in $F_{net,sol}$ of more than $80\,W\,m^2$ between the model an the observations. Due to relatively large amount of observations being present for that day, this effect of this day can also be seen in Figure 2. Therefore, this narrower range of $F_{net,sol}$ can be considered to be both, a model and a sampling bias. It is exactly for that reason why we filtered both datasets so that they are in the same radiative state.

13. Fig 5: I personally find it hard to draw quantitative conclusions from this plot going beyond the overall range of values in observations and simulations. You can sort of see that geometrical cloud

depth is likely underestimated, but its hard to tell due to the many overlapping points where the real density of points is. As suggested previously, I wonder if a PDF comparison would not be more informative
Depicting the bias in geometrical cloud depth in a histogram is indeed a good idea and we revised Fig. 5 accordingly.

14. Fig. 6-8: Panel a): I am fairly sure the ICON and ACLOUD lines are swapped? Otherwise there would be a mismatch between your figure and the discussion and the results of sections 4.2ff. Panel b): The ACLOUD in Fig6 is slightly different to 7/8. Why?
Thanks for spotting that issue, the lines in Fig. 6-8: Panel a) are indeed swapped. This has been corrected in the revised manuscript. As discussed for radiative properties, the cloud field is different between the different sensitivity studies. As only datapoints are being used when both, the model and the observation, are within a cloud at the same time, the histograms do slightly differ. This is clarified in the revised manuscript.

15. Fig. 9: Ultimately the net cloud-radiative effect is of interest, but your argument primarily relates to CREsol. What is the impact of CREsol alone?
The CRE is mainly mediated by its solar component in all the sensitivity studies. The terrestrial components are in good agreement with the observationally derived terrestrial CRE components. We included this information to the revised manuscript and included the respective figures in a supplement to the article.

16. Table 1: I personally would find a a total number of included flight hours as part of the caption helpful.
A total of approx. 116 flight hours has been used for this comparison. We added this information to the caption.

Edits

1. L165: suggested rephrase "to the previous comparison" to "to the previously used model setup".
2. L248: "the the"
3. L291: suggest rephrase "than observed the mean of" to "than the observed mean of"
4. L423: Typo? Underestimation of geometrical cloud depth, right?
5. L424: "represent" instead of "simulate" (since you do not really simulate it)
All remarks have been implemented as proposed.

Further revision

In line 186 of the submitted manuscript, the threshold for a surface to be classified as sea ice covered should be 0.7, not 0.5. This has been corrected in the revised manuscript.

References

Morrison, H. and Pinto, J. O.: Mesoscale Modeling of Springtime Arctic Mixed-Phase Stratiform Clouds Using a New Two-Moment Bulk Microphysics Scheme, Journal of the Atmospheric Sciences, 62, 3683–3704, https://doi.org/10.1175/JAS3564.1, 2005.

Raschendorfer, M.: The new turbulence parameterization of LM, COSMO newsletter No. 1, pp. 89–97, 2001.

Response to referee comment #2

In this paper, the authors compare simulations using the ICON model to observationsfrom the ACLOUD and PASCAL campaigns. They find that the ICON simulations predict a more strongly positive cloud radiative effect (CRE) than that derived from the ACLOUD observations. They then determine that an important contribution to this difference is the small number of cloud condensation nuclei (CCN) activated in the ICON model, which subsequently results in low cloud liquid water contents. They improve the model results by accounting for the effects of subgrid-scale turbulence on cloud droplet activation and by scaling their assumed CCN profile. I feel that the study merits publication, provided that the following comments are addressed.

We thank the reviewer for the constructive comments that helped to improve the manuscript.

General comments

1. The authors briefly mention cloud ice in a few places in the paper, but they largely restrict their analysis to liquid cloud water. Some definitive or quantified statements about the contributions of ice clouds to the radiation balance or hydrometeor concentrations, both in ICON and in the observations, would be welcome. Could differences in the amount of frozen cloud make a significant contribution to differences in the surface radiation balance or the cloud radiative effect between the model and the observations?

From the observational side, it is difficult the quantify contribution of ice clouds to the radiation balance or hydrometeor concentrations as the amount of ice in the clouds during ACLOUD and especially during the period of our sensitivity study was relatively low and often times below the detection threshold of the in-situ probes. Looking at the ICON model, we have performed a sensitivity analysis in which we turned off any radiative effect of cloud ice. If one compares the radiative variables like surface CRE (see Figure 1 and Figure 2) and F_{net} at the surface (not shown), the differences between our basic set up of ICON and the one without an effect of cloud ice on the radiative field is small and on the order of 1 $W\,m^{-2}$. This is due to the already low cloud ice fraction in the model, which also causes the radiative effect of cloud ice to be low. Due to the limitations of the observational dataset in terms of cloud ice, it is hard to constrain the model from the observational side. Therefore, any estimation of the impact of cloud ice on the radiative balance has to be interpreted with some caution. We added this information to the revised manuscript.

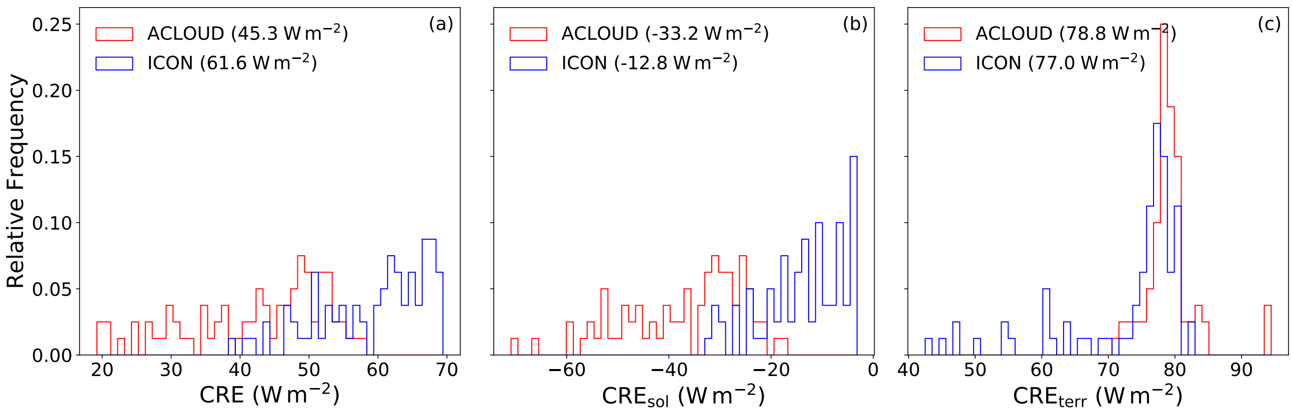

Figure 1: As Fig. 4 in the revised manuscript but for the period from 2 June to 5 June.

2. Sect. 3.2, p9: The authors mention here that the CRE is calculated from the observations through the methods of Stapf et al. (2019a). Given that there are potential inconsistencies in the calculated CRE between the model and the observations, just a little more detail on the radiative transfer simulations of Stapf et al. (2019a) seems prudent here.

In the revised manuscript, more information on the radiative transfer simulations are given.

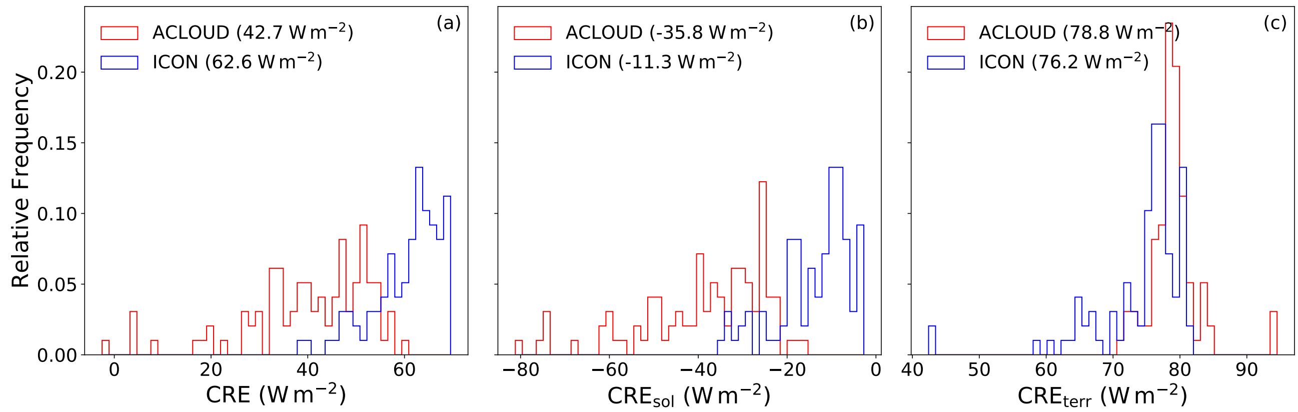

Figure 2: As Fig. 4 in the revised manuscript but for the period from 2 June to 5 June and without effect of cloud ice on radiation.

The authors mention that "While the prescribed functional dependence of the sea ice albedo has been derived for cloudless and cloudy conditions, the surface albedo that is used to derive the CRE from the observations is for cloudy-sky only. This can lead to inconsistencies between the modeled and observed CRE (Stapf et al., 2019a)." However, If I understand correctly, the radiative transfer simulations of Stapf et al. (2019a) account for cloud surface-albedo interactions. Given that the surface albedo is prescribed in the ICON simulations, these cloud-surface-albedo interactions will not be accounted for in the ICON simulations. Therefore, wouldn't it be a more consistent comparison if the cloud-surface-albedo interactions were also neglected in CRE calculations based on the observed data? Can the authors comment on this?
The radiative transfer simulations to derive the CRE from the observation are different from the ones in Stapf et al. (2019a) as in our study, the albedo from all-sky conditions was used. All-sky albedo was also used to derive the functional dependency used that we implemented into ICON for the purpose of this study. We now explicitly state that all-sky albedo was used and removed a misleading citation to Stapf et al. (2019a) to avoid confusion.

Specific comments and technical corrections

p2, line 38: optical → optically
Changed.

p2, lines 44-47: Please improve the clarity of this sentence.
Following the advise by reviewer #1 to reduce the LES vs kilometer-scale simulation, this sentences has been removed in the revised manuscirpt.

p3, line 74: sea ice covered → sea-ice-covered
Changed.

p3, line 83: unmatched parenthesis: "given (for"
Parenthesis added.

p3, line 84: refer → refer the reader to
Changed.

p5, line 108: "general feature of ICON." Perhaps the authors mean "generally representative of ICON"?

Changed.

p5, line 120: "caused by the way how our simulations" Please either choose "the way that" or "how".
Changed to "how".

p8, line 176 "sea ice covered surface". This should be either "the sea-ice-covered surface" or "sea-ice-covered surfaces".
Changed to "sea-ice-covered surfaces".

p8, line 189: "Figure 3 a" → "Figure 3a"
We refer to Figure 3a in the following sentence, and this sentence was intended to generally introduce this figure.

p9, line 200: Please insert a comma after "without clouds"
Comma inserted.

p9, line 202: "measurements of atmospheric/surface observations". Perhaps the authors mean "atmospheric or surface measurements" or "atmospheric or surface observations"?
Here, we refer to observatoins of the atmosphere (i.e. dropsonds) and of surface properties (i.e. albedo). We reformulated this sentence to be more concise.

p9, line 211: Please either choose "The way that" or "How".
Changed to "The way that".

p9, line 212: "allows to narrow down, which effect" → either "allows us to narrow down which effect" or "allows one to narrow down which effect".
Changed to "allows us to narrow down which effect".

p9, line 212: "If clouds would be" → "If clouds were"
Changed.

p9, line 215: "fraction" → "ratio"
Changed.

p10, line 226: "which allows to" → "which allows us to"
Changed.

p11, line 260: "extend" → "extent"
Changed.

p13, line 301: large → larger
Changed.

p13, line 302: stems → stem
Changed.

p14, lines 327-328:The overestimation of small hydrometeors mentioned here seems to be in contradiction to the statements of p12, lines 278-280.
Here, we refer to the overestimation of small hydrometeors in Schemann and Ebell (2020). Due to the much finer resolution of their ICON simulations, the activation of CCN into cloud droplets can be sufficiently resolved and any bias is only to the unsuited background CCN profile for an Arctic domain. Neverthless, we revised this sentence to make that clearer that we refer to the simulations in Schemann and Ebell (2020).

p16, lines 393-394: Since the last simulation discussed was not the default set-up but instead was the one using the revised CCN activation scheme, most readers would assume that the authors are comparing the simulation with the CCN scaled by 0.4 to the revised CCN activation simulation. The authors need to make it clear that they are comparing this simulation to the default set-up.
It has been clarified in the revised manuscript that we scaled the revised CCN activation simulation and not the default set-up.

p17, lines 411 and 414: Do the authors mean Figure 9f instead of 9e?
Yes indeed, Figure 9f is the one we refer to. This has be changed accordingly.

p20, eq. B3: If I divide eq. B2 with $k = 3$ by eq. B2 with $k = 2$, I find the trailing factor to be $A^{-1/\mu}$, not $\lambda^{-1/\mu}$. Is the error in eq. B2 or eq. B3?
Thanks for thoroughly going through the equations. Indeed, there is a typo in B2 as there has to be a λ in the denominator instead of A. This has been corrected in the revised manuscript.

Figure 1 caption: "inner domain has a" → "inner domain (red) has a"
Changed as proposed.

Figure 5 and p11, lines 258-261: There is significant overlap in the points on this plot, which makes it difficult to tell, for example, how large a fraction of the data have observed cloud depth < 0.4 and modelled cloud depth < 0.2. This also means that it is difficult to judge the degree of underestimation of the cloud depths. I don't have a perfect solution for this issue, but the authors may wish to consider making the data points partially transparent, or substitution of the scatter plot with a histogram (with different subplots for the different observation days, if the authors wish). I am open to other solutions, or arguments from the authors in favour of the current plot. In any case, the median values of the modelled and observed cloud depths should be provided to help the reader quantify the degree of underprediction. The means and standard deviations may also be helpful.
We revised this figure and now display the bias in the form of a histogram. The mean and the standard deviation of the depicted histogram are given in the revised manuscript.

Figure 6, Figure 7, and Figure 8: The red lines for panels b and c are very similar in the three figures, but not quite identical. Note for instance that the peak in frequency of hydrometeor number concentration is > 100 in Figure 6 and < 100 in Figure 7 and Figure 8. Rather than state in the captions that the lines are identical, the authors instead should very briefly remind the reader why the lines differ slightly. Also, it seems that the red and blue lines are reversed in panel a in all three figures.
The lines in Fig. 6-8: Panel a) are indeed swapped, which has been corrected in the revised manuscript.

Figure 9: It would be prudent to remind the reader in the caption that the red lines differ slightly due to the sampling that is applied.
We added a remark in the caption of Figs. 6-9 that the red lines differ due to the sampling strategy employed.

Further revision

In line 186 of the submitted manuscript, the threshold for a surface to be classified as sea ice covered should be 0.7, not 0.5. This has been corrected in the revised manuscript.

References

Schemann, V. and Ebell, K.: Simulation of mixed-phase clouds with the ICON large-eddy model in the complex Arctic environment around Ny-Ålesund, Atmospheric Chemistry and Physics, 20, 475–485, https://doi.org/10.5194/acp-20-475-2020, 2020.

Employing airborne radiation and cloud microphysics observations to improve cloud representation in ICON at kilometer-scale resolution in the Arctic

Jan Kretzschmar[1], Johannes Stapf[1], Daniel Klocke[2,3], Manfred Wendisch[1], and Johannes Quaas[1]

[1]Institute for Meteorology, Universität Leipzig, Leipzig, Germany
[2]Deutscher Wetterdienst, Offenbach, Germany
[3]Hans-Ertel-Zentrum für Wetterforschung, Offenbach, Germany

Correspondence: Jan Kretzschmar (jan.kretzschmar@uni-leipzig.de)

Abstract. Clouds play a potentially important role in Arctic climate change, but are poorly represented in current atmospheric models across scales. To improve the representation of Arctic clouds in models, it is necessary to compare models to observations to consequently reduce this uncertainty. This study compares aircraft observations from the Arctic Cloud Observations Using Airborne Measurements during Polar Day (ACLOUD) campaign around Svalbard, Norway in May/June 2017 ~~around Svalbard, Norway - to~~ and simulations using the ICON (ICOsahedral Non-hydrostatic) model in its numerical weather prediction (NWP) set-up at 1.2 km horizontal resolution. By comparing measurements of solar and terrestrial irradiances during ACLOUD flights to the respective properties in ICON, we showed that the model systematically overestimates the transmissivity of the mostly liquid clouds during the campaign. This model bias is traced back to the way cloud condensation nuclei (CCN) get activated into cloud droplets in the two-moment, bulk microphysical scheme used in this study. This process is parameterized as function of grid-scale vertical velocity in the microphysical scheme used, but in-cloud turbulence cannot sufficiently be resolved at 1.2 km horizontal resolution in Arctic clouds. By parameterizing subgrid-scale vertical motion as a function of turbulent kinetic energy, we are able to achieve a more realistic CCN activation into cloud droplets. Additionally, we showed that by scaling the presently used CCN activation profile, the hydrometeor number concentration could be modified to be in better agreement with ACLOUD observations in our revised CCN activation parameterization. This consequently results in an improved representation of cloud optical properties in our ICON simulations.

1 Introduction

In recent decades, the Arctic has proven to be especially susceptible to global climate change (Screen and Simmonds, 2010), as several positive feedback mechanisms strengthen the warming in high latitudes of the Northern Hemisphere ~~(Serreze and Barry, 2011)~~ (Serreze and Barry, 2011; Wendisch et al., 2017). Among those feedback mechanisms that influence the Arctic climate, the cloud feedback - even though being small in magnitude compared to other feedback mechanisms like the surface albedo or temperature feedbacks - exhibits a relatively large uncertainty (Pithan and Mauritsen, 2014; Block et al., 2020). This uncertainty can be related to the general complexity of the Arctic climate system and to misrepresented microphysical processes in global climate models (GCMs) that are used to quantify the cloud feedback. Typical issues associated with the simulation of clouds in the Arctic are incorrectly simulated amount and distribution of clouds (English et al., 2015; Boeke and Taylor, 2016), which often can be linked to an erroneous representation of mixed-phase clouds (Cesana et al., 2012; Pithan et al., 2014; Kretzschmar et al., 2019). This consequently affects the quantification of the effect of Arctic clouds on the (surface) energy budget in GCMs (Karlsson and Svensson, 2013).

To identify processes within the microphysical parametrization that are misrepresented in models, it is inevitable to compare them to appropriate observations (Lohmann et al., 2007). As pointed out by Kay et al. (2016), any comparison between modeled and observed quantities can easily be misleading if it is not scale- and definition-aware. For GCMs, observations from satellite remote sensing are well suited, being on similar scales as those large scale models. A comparison to ~~satellite derived~~ satellite-derived quantities can further be made definition-aware by using instrument simulators like they are provided within the Cloud Feedback Model Intercomparison Project's (CFMIP) Observation Simulator Package (COSP; Bodas-Salcedo et al., 2011). The benefit of using COSP for evaluating clouds in GCMs in the Arctic has been shown in several studies (Barton et al., 2012; Kay et al., 2016; Kretzschmar et al., 2019).

Even though satellite observations provide valuable information on the atmospheric state in the Arctic, they often suffer from ~~instrument dependent~~ instrument-dependent idiosyncrasies like ground clutter for a space-borne cloud radar or attenuation of the beam of a space-borne lidar by ~~optical~~ optically thick clouds (Cesana et al., 2012). Those problems can be in part overcome by using ground-based or aircraft observations. Due to much smaller temporal and spatial scales, those observations only have limited suitability for the evaluation of large-scale models. To this end, the use of storm-resolving models with grid sizes on the order of kilometers or large eddy models is necessary, as they are able to better capture features and variability present in those rather smaller scale observations (Stevens et al., 2019). Due to the relatively large computational effort that is needed for large eddy simulations, they are limited in spatial extent and ~~, for that reason,~~ are often used for comparison with ground based observations at individual locations in the Arctic ~~(Loewe et al., 2017; Sotiropoulou et al., 2018; Neggers et al., 2019; Schemann and Ebell, 2020~~ ~~. If one wants to use aircraft observations of the Arctic atmosphere to compare it to models, the computational resources needed for such a comparison can be a limiting factor to perform such highly resolved simulation, especially when multiple days should be considered. Nevertheless, a comparison of large eddy simulations to aircraft observations for well-defined situations can give valuable insights into physical processes within the Arcticatmosphere. Such simulations can be particularly useful when the high resolution of a large eddy set-up is explicitly needed to allow for a comparison with small scale phenomena like in-cloud turbulence (Mech et al., 2020) or cloud-top inhomogeneity (Schäfer et al., 2018; Ruiz-Donoso et al., 2020) that are observed from the airborne remote sensing~~(e.g. Loewe et al., 2017; Sotiropoulou et al., 2018; Neggers et al., 2019; Schemann and Ebell, 2020) . Furthermore, large eddy simulation have been used to study and evaluate microphysical processes (e.g. Fridlind et al., 2007; Ovchinnikov , as well as aerosol-cloud interactions (e.g. Possner et al., 2017; Solomon et al., 2018; Eirund et al., 2019) in the Arctic. To avoid the need for large computational resources but still be able to resolve many processes that act on scales that cannot be captured by GCMs, limited area simulations with grid sizes on the order of a few kilometers, where (deep) convection does not need to be explicitly parameterized, can offer a good compromise. Simulations at such resolutions on relatively large domains have received increased interest in recent years (Stevens et al., 2019).

This study makes use of such a set-up using the ICOsahedral Non-hydrostatic (ICON) model (Zängl et al., 2015) at kilometer-scale horizontal resolution. Studies, mainly focusing on the tropical Atlantic, have ~~shown~~ reported that the model at storm-resolving resolutions is able to simulate the basic structure of clouds and precipitation in that region (Klocke et al., 2017; Stevens et al., 2020). In the present study, ICON is used in a similar set-up and is compared to observations that have been derived from the Arctic Cloud Observations Using Airborne Measurements during Polar Day (ACLOUD) campaign ~~in May/June 2017~~ around Svalbard, Norway (Wendisch et al., 2019; Ehrlich et al., 2019) ~~. This study~~ and to observations derived during the Physical Feedbacks of Arctic Boundary Layer, Sea Ice, Cloud and Aerosol (PASCAL; Flores and Macke, 2018) ship-borne observational campaign in the sea ice covered ocean north of Svalbard in May and June 2017. This study mainly compares observations of solar and terrestrial irradiances during ACLOUD flights to our ICON simulations to obtain a first estimate whether the model is able to correctly simulate general cloud optical properties. Based on the results of this comparison, it is further explored to what extent cloud macro- and microphysical properties might be misrepresented in this set-up and how to improve the simulation of clouds in ICON at kilometer-scale.

2 Data and model

2.1 ACLOUD/PASCAL campaign

In May and June 2017, two concerted field studies took place around Svalbard, Norway (Wendisch et al., 2019): the Arctic Cloud Observations Using Airborne Measurements during Polar Day (ACLOUD; Ehrlich et al., 2019) campaign and the Physical Feedbacks of Arctic Boundary Layer, Sea Ice, Cloud and Aerosol (PASCAL; Flores and Macke, 2018) ship-borne observational study. The airborne measurements during ACLOUD where conducted with the two research aircraft Polar 5 and Polar 6 (Wesche et al., 2016) that were based in Longyearbyen (LYR), Norway. While Polar 5 focused on remote sensing observations of mainly low-level clouds and surface properties from higher altitudes (2-4 km), Polar 6 concentrated on in situ observations of cloud microphysical and aerosol properties, in and below the clouds. Ground-based observations from the ship and an ice floe in the ~~sea ice covered~~ sea-ice-covered ocean north of Svalbard were performed during PASCAL using the German research vessel (R/V) Polarstern (Knust, 2017). Additionally, a tethered balloon was operated on an ice floe camp during PASCAL (Egerer et al., 2019).

The synoptic development during both campaigns is separated into three phases (Knudsen et al., 2018). A period with advection of cold and dry air from the north in the beginning (23-29 May 2017) was followed by a warm and moist air intrusion into the region where the two campaigns took place (30 May -12 June 2017). During the final two weeks of the campaigns (13-26 June 2017), a mixture of warm and cold ~~airmasses~~ air masses prevailed. Especially during the last two phases, clouds in the domain close to Polarstern, where the bulk of the measurements took place, mainly consisted of (super-cooled) liquid clouds with only little cloud ice being present (Wendisch et al., 2019).

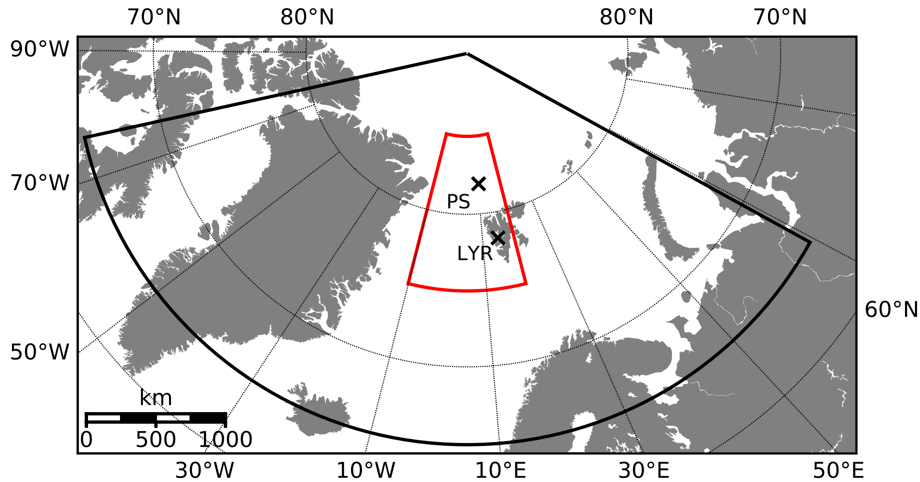

Figure 1. Set-up of the limited-area simulations. The outer domain (black) has an approximate resolution of 2.4 km, while the inner domain (red) has a resolution of 1.2 km. Additionally marked is Longyearbyen/Norway (LYR) where Polar 5 and Polar 6 were stationed during ACLOUD, as well as the postion of the R/V Polarstern (PS) during the ice floe camp.

In the following, a brief description of the instrumentation and data used in this study is given (for a comprehensive overview we refer the reader to Wendisch et al. (2019) and Ehrlich et al. (2019)). Two pairs of upward and downward looking CMP 22 pyranometers for the solar (0.2-3.6 μm) and CGR4 pyrgeometers for major parts of the terrestrial spectral range (4.5-42 μm) were installed on board of Polar 5 and Polar 6 to measure the upward and downward broadband (solar and terrestrial) irradiances on both aircraft (Stapf et al., 2019). We also utilize microphysical data that have been derived from in-situ measurements on Polar 6. We use data of the particle size number distribution obtained from the Small Ice Detector Mark 3 (SID-3) (Schnaiter and Järvinen, 2019) covering a size range of 5-45 μm divided into 16 size bins (2-5 μm resolution). For more information on the SID-3 and processing of the measurements, the reader is referred to Schnaiter et al. (2016) and Ehrlich et al. (2019). For comparison of the bulk liquid water content, we exploit data from a Nevzorov probe (Korolev et al., 1998) that was installed on Polar 6 (Chechin, 2019). Furthermore, we use observations of cloud base height as observed by the laser ceilometer and cloud top height derived from a 35 GHz cloud radar (Griesche et al., 2019) onboard R/V Polarstern to derive geometrical cloud depth in the sea ice-covered ocean north of Svalbard.

2.2 ICON simulations

In this study, data measured during ACLOUD and PASCAL ~~is~~ are compared to the output of the ICOsahedral Non-hydrostatic model (ICON; Zängl et al., 2015). ICON is a unified modelling systems that allows simulations on several spatial and temporal scales, spanning from simulation of the global climate on the one end (Giorgetta et al., 2018) to high resolution large eddy simulations (LES) on the other (Dipankar et al., 2015; Heinze et al., 2017). ICON is also employed as a numerical weather prediction (NWP) model at the German Meteorological Service (Deutscher Wetterdienst, DWD). For each application (GCM, NWP, LES), a dedicated package of physical parametrizations is provided to satisfy the specific needs for each set-up. For our simulations, the applied set of physical parametrizations is similar to that used in Klocke et al. (2017). However, we use the two-moment, bulk microphysical scheme developed by Seifert and Beheng (2006) instead of the single moment scheme by Baldauf et al. (2011) used in Klocke et al. (2017). Furthermore, we apply an all-or-nothing cloud cover scheme that allows for grid-scale clouds only as this facilitates the comparison with the observations. At the resolutions used in this study, an all-or-nothing cloud cover scheme might miss some clouds as the necessary saturation humidity might not be reached. A comparison to simulations with a fractional cloud cover scheme showed only little differences compared to the all-or-nothing cloud cover scheme used, which made us confident that resolving clouds at grid scale only is sufficient for our set-up. The Rapid Radiation Transfer Model (RRTM; Mlawer et al., 1997) is applied to derive the radiative fluxes. Due to the rather fine horizontal resolution of our simulations, we only parametrized shallow convection using the Tiedtke (1989) shallow convection parameterization with modifications by Bechtold et al. (2008), whereas deep convection is considered resolved (albeit not relevant for the Arctic case considered here). In the following, the used set-up will be simply denoted as ICON. However, findings in this study are specific to our chosen set-up (spatial scale and parameterizations used) and should not be seen as ~~general feature of~~ generally representative for ICON.

We deploy ICON in a limited-area set-up with one local refinement (nest) in the region where the research flights and ship observations were performed (Figure 1). The outer domain has a horizontal resolution of approximately 2.4 km (R2B10 in the triangular refinement) while the inner nest has a refined resolution (R2B11) of approximately 1.2 km. For both domains, we use 75 vertical levels spanning from the surface to 30 km altitude with a vertical resolution of 20 m at the lowest model level that gradually gets coarser towards model top. We initialize the model using the analysis of European Center of Medium Weather Forecast (ECMWF) Integrated Forecasting System (IFS). The respective IFS forecast is used as boundary data to which we nudge our model every three hours. We do not continuously run the model for the whole period of the campaign but re-initialize the model from the 1200 UTC analysis of the previous day in case of a subsequent day with flight activities. This gives the model a spin-up time of more than 12 hours even for takeoffs in the early morning.

During the initial comparison of ICON and the ACLOUD observations, we found that the albedo of sea ice in the model is substantially lower compared to values observed during ACLOUD (Wendisch et al., 2019). The reason for this underestimation of the surface albedo in ICON is caused by ~~the way~~ how our simulations are initialized using the IFS analysis. As the IFS sea ice albedo is not used during the initialization of ICON, the parametrization of the sea ice albedo performs a cold start. For such a cold start, the sea ice albedo is ~~only~~ a function of the sea ice surface temperature only, as given by Mironov et al. (2012) (their Equation 5). This formulation was slightly adapted in ICON by setting the maximum sea ice albedo (α_{max}) to 0.70 and the minimum sea ice albedo (α_{min}) to 0.48. For surface temperatures close the freezing point (as it has been observed during ACLOUD, especially in the second half of the campaign), such a cold start results in albedo values that are considerably lower compared to the observations. This underestimation of the sea ice albedo could be avoided by increasing the spin-up of the model to a few weeks or by using DWD ICON analysis instead of the IFS analysis. In the latter case, the albedo is initialized from the initial data and no spin-up is required (Wendisch et al., 2019). As one of the main aims of this comparison are ~~radiative fluxes~~irradiances, an accurate representation of surface albedo is crucial and we, therefore, chose to take yet another approach.

For each day, we use prescribed values for Due to the fact that the simulated period falls into the onset of the melting period, the sea ice albedo that are derived from the aircraft observationssignificantly reduces in that period. To accurately represent this reduction in sea ice albedo, we prescribe the sea ice albedo as a function of time to be consistent with the observed sea ice albedo. For this purpose, from the observations, only scenes with homogeneous sea ice are selected using a fish-eye-camera-derived sea ice concentration threshold of 95 %. The daily averaged observed albedo is parameterized as a function of day of the year and is held constant for any specific day. This approach by construction results in a standard deviation of as little as 0.024 between daily modeled and observed albedo. In case of fractional sea ice cover in the model, the surface albedo is a surface fraction-weighted average between the prescribed value and the albedo of open water (taken as 0.07).

For the comparison of our ICON simulations to the ACLOUD data, we temporally and spatially collocate the model output to be consistent with the actual position and altitude of the aircraft. We use a multidimensional binary search tree (also known as k-d tree; Bentley, 1975) to sample the model output along the flight track in space and time directly on its native unstructured, triangular grid. The temporal frequency of the observational data is 1 Hz. Additionally, we averaged the (sampled) datapoints from the observations and the simulations into 20 second intervals. This ensures that the observational data is on a similar spatial scale as the simulation on the 1.2 km grid of the inner domain (considering an average velocity of the aircraft of $60\,\mathrm{m\,s^{-1}}$). Due to storage constraints, we chose to output the model state only every 30 minutes, which reduces temporal variability in the model output. As the planes are not static and "fly" through the model grid, temporal variability is, to some extent, replaced by spatial variability when sampling a large enough large-enough area along the flight track. Additionally, the 30 minute output frequency introduces inconsistencies in the top of atmosphere incoming solar irradiance, as the solar zenith angle is constant in the model output while it varies with time in the observationswithin those 30 minute intervals. This implies that the largest temporal difference between an observational data point and the output timestep of ICON is ± 15 minutes, causing a bias of up to $\pm 14\,\mathrm{W\,m^{-2}}$ for incoming solar irradiation at the top of the atmosphere in the early morning and late evening when the temporal derivative of incoming solar radiation is the largest. As most of flights took place during noon and we mostly focus on cloudy conditions, we expect this bias to be on the order of a few $\mathrm{W\,m^{-2}}$ at most, making us confident that this issue will not significantly influence the overall findings in this study. Even though being on similar scales, spatial and temporal variability in both datasets prohibit a one-to-one comparison. We will, therefore, mainly use histograms in the comparison.

3 Surface radiative quantities as simulated with ICON and measured during ACLOUD

In the following, the simulations are compared to data for several surface radiative variables that have been observed during low-level flight sections. Some flights were excluded due to relatively short flight times to save computational resources. Additionally, some flights with cloudless conditions towards the end of the campaign were excluded not analyzed as the main focus of this study is a comparison of cloud properties. An overview of the flights used for the comparison is given in Table 1. In the observation and in the model, we define low-level flight sections as such that no cloud is present below the present altitude of the aircraft.

Table 1. Flights used for the comparison to ICON simulations (approximately 116 flight hours). The values given for the low-level scenes corresponds to the number of the averaged 20 second intervals used in the following comparison. For more information on the scientific target of each research flight, refer to Wendisch et al. (2019) and Ehrlich et al. (2019).

Flight No.	Date in 2017	Flight Time (UTC)		Low-level scenes	
		Polar 5	Polar 6	all-sky + all surfaces	cloudy + sea ice
4	23 May	09:12-14:25	-	69	12
5	25 May	08:18-12:46	-	-	-
6	27 May	07:58-11:26	-	-	-
7	27 May	13:05-16:23	13:02-16:27	58	-
8	29 May	04:54-07:51	05:11-09:17	60	-
10	31 May	15:05-18:57	14:59-19:03	199	-
11	2 June	08:13-13:55	08:27-14:09	73	7
12	4 June	-	10:06-15:39	65	55
13	5 June	10:48-14:59	10:43-14:44	101	70
14	8 June	07:36-12:51	07:30-13:20	80	6
17	14 June	12:48-18:50	12:54-17:37	275	275
18	16 June	04:45-10:01	04:40-10:31	-	-
19	17 June	09:55-15:25	10:10-15:55	95	22
20	18 June	12:03-17:55	12:25-17:50	131	-
23	25 June	11:09-17:11	11:03-16:56	347	-

3.1 Spatial structure of the radiative field of the Arctic atmospheric boundary layer

In the Arctic, two distinct radiative states have been reported: a radiatively clear state with no, or only radiatively thin clouds and a cloudy state with opaque clouds (Shupe and Intrieri, 2004; Stramler et al., 2011). This two-state structure was also observed during ACLOUD, but compared to spatially fixed observations with almost constant surface albedo, observations during ACLOUD were further decomposed into a cloudy and cloudless state over sea ice and open ocean, which consequently results in a four-state structure (Wendisch et al., 2019). As in Wendisch et al. (2019), we compiled two-dimensional histograms of surface albedo and surface net terrestrial ~~/net solar irradiance, which is~~ and net solar irradiances, defined as the difference between downward and upward radiative energy flux densities, for the ACLOUD observations and the ICON simulations

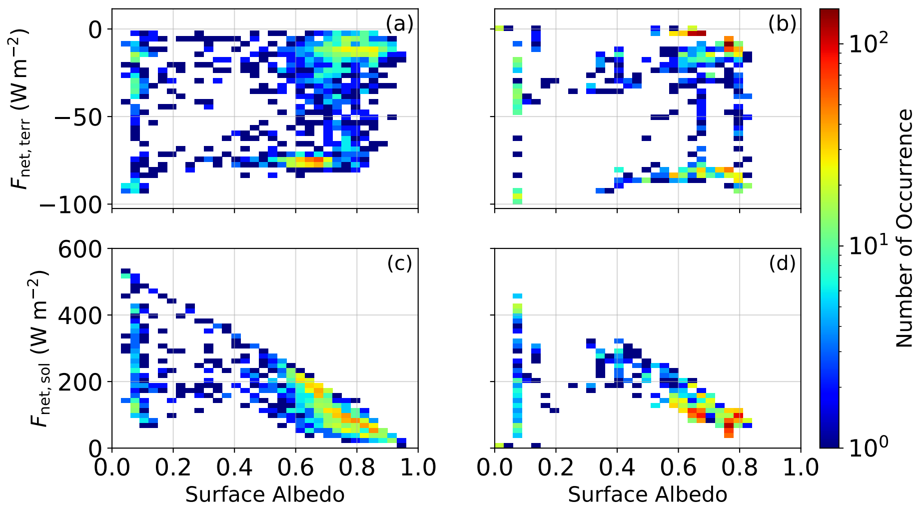

Figure 2. Two dimensional histograms of surface albedo and (top row; a, b) net terrestrial-/ (bottom row; c, d) net solar irradiance at the surface (W m^{-2}) for (left column; a, c) ACLOUD observations and (right column; b, d) ICON simulations.

(Figure 2). The general difference to Wendisch et al. (2019) (their Figure 14) is explained by the prescribed surface albedo approach applied in this study, which results in higher sea ice albedo values compared to the ~~previous comparison~~previously used model set-up.

In general, the structure of the modeled net terrestrial irradiance ($F_{\mathrm{net,terr}}$) close to the surface (Figure 2 ~~a/b)~~(a) and (b)) is in agreement with the observed one. Only for surface albedo values between 0.6 and 0.7, noticeable differences between the ACLOUD observations and the ICON simulations become obvious. Those albedo values are related to days towards the end of the campaign (mid/late June 2017) when the melting season had begun and sea ice albedo was reduced. For this period, the model overestimates the presence of cloudy conditions whereas cloudless conditions were present in the ACLOUD observations. Conversely, for situations with sea ice albedo greater than 0.7, ICON overestimates the presences of cloudless conditions. The lack of cloudless conditions for surface albedo values between 0.6 and 0.7 in the ICON simulations is also visible from the histograms of surface albedo and net solar irradiance (Figure 2 ~~c/d)~~(c) and (d)). For surface albedo larger than 0.7, the net solar irradiance ($F_{\mathrm{net,sol}}$) close to the surface seems, on average, ~~to be~~ in agreement with the observations, even though the observed variability in surface albedo is not simulated by the model. The reported discrepancies can be influenced by the input used to force our limited-area simulations. This can be seen in the underestimation of the albedo of sea ice covered surface despite the prescribed surface albedo in the model that is in accordance with the observed sea ice albedo. This bias is, therefore, related to differences in sea ice fraction in the model and in the observation and indicates that the sea ice fraction in the ECMWF input data is too small.

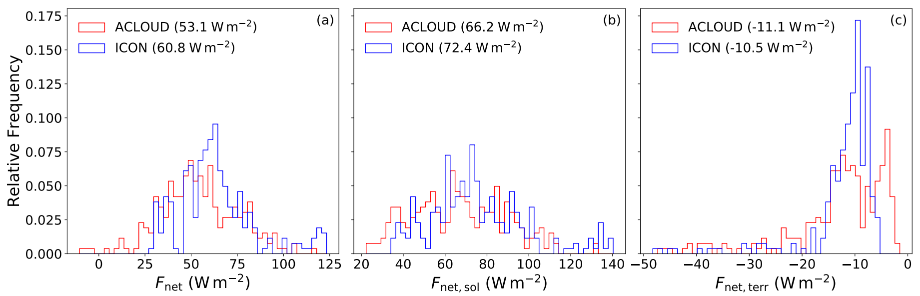

Figure 3. Relative frequency distributions of (blue) modeled and (red) observed surface net irradiation for sea-ice covered surfaces and cloudy conditions for (a) total radiation, (b) solar, and (c) terrestrial radiation. Values in the legend indicate the median of the respective variables.

3.2 Surface net irradiances and cloud radiative effect over sea ice and below clouds

This section explores the effect of clouds on the surface radiative budget in the ACLOUD observations and in our ICON simulations over sea ice. For that purpose, we, at first, look at net surface irradiance, which we further split into its solar and terrestrial components. To ensure comparability, despite obvious differences between the ICON simulations and ACLOUD observations described in subsection 3.1, we will restrict our comparison to situations where the model and the observations are within the same cluster of the two-dimensional histograms of surface albedo and surface net terrestrial irradiance at the same time. To distinguish between those clusters, a situation is defined as cloudy if the net terrestrial irradiance at the surface is larger than -50 W m^2~~and~~. Furthermore, a surface is classified sea ice covered, if the surface albedo is larger than ~~0.5~~0.7 but less than 0.85, which is equivalent to the daily averaged maximum albedo value used in our adapted albedo parameterization. As we are interested in cloud (radiative) properties over sea ice covered surface, we will focus our evaluation on those situations. Furthermore, this cluster is appealing as most low-level flight sections were performed under these conditions.

In Figure 3, we compare observed and simulated net near surface irradiances using histograms. From Figure 3a, it becomes obvious that the model systematically overestimates net surface irradiances below clouds and over sea ice. This variable also shows a quite strong variability for both the model and the observations, which is related to varying sea ice albedo during the campaign. Additionally, the incoming solar radiation varied between research flights as they took place at different times of the day, which also introduces further variability. Looking at medians of the spectral components, we find that differences between simulated and observed net surface irradiances are mainly mediated by its solar component, while the median of net terrestrial surface irradiances are well simulated by ICON and also the shape of their histograms match better. Besides the above reported underestimated surface albedo for sea ice covered surface in ICON, also misrepresented cloud optical properties can contribute to the positive bias in net solar irradiances at the surface.

Furthermore, we investigate the surface cloud radiative effect (CRE) during ACLOUD, which is defined as the difference between net surface irradiance for cloudy and cloudless conditions. In the model, cloudy and cloudless irradiances can easily be derived by a double call to the radiation routines, one with clouds and one without clouds, leaving all variables not related to clouds constant. For observations, it is impossible to simultaneously observe both cloudy and cloudless conditions. Therefore, irradiances of cloudless conditions were obtained from dedicated radiative transfer simulations ~~based on measurements of atmospheric~~ that used observations of atmospheric (i.e. temperature/~~surface observations (Stapf et al., 2020). While the prescribed functional dependence of the sea ice albedo has been derived for cloudless and cloudy conditions, the surface albedo that~~ humidity profiles) and surface properties (albedo). The one-dimensional, plane-parallel discrete ordinate radiative transfer solver DISORT (Stamnes et al., 1988) included in the libRadtran package (Emde et al., 2016) was applied for this purpose. The molecular absorption parameterizations from Kato et al. (1999) for the solar spectral range (0.28-4 μm) and from Gasteiger et al. (2014) for the terrestrial wavelength range (4-100 μm) were chosen. For calculating the observationally based CRE, the observed all-sky albedo was used, which also is used to ~~derive the CRE from the observations is for cloudy-sky only. This can lead to inconsistencies between the modeled and observed CRE (Stapf et al., 2020).~~ create the prescribed functional dependency of the sea ice albedo that has been applied in the ICON model. Potential inconsistencies regarding the surface-albedo-cloud interaction and related issues discussed in Stapf et al. (2020) (they applied cloudless albedo estimates) are thus avoided. Unavoidable uncertainties in the comparison caused by the different applied radiative transfer schemes remain possible

The overwhelming majority of the observed and modeled total (solar plus terrestrial) surface CRE values are positive over sea ice, which indicates that clouds have a warming effect on the surface (Figure 4a). This is consistent with the relatively high surface albedo values at the onset of the melting period during ACLOUD (Jäkel et al., 2019; Wendisch et al., 2019), which decreases the cooling effect of clouds in the solar spectral range. Similar to the net surface irradiance, ICON overestimates the total surface CRE (Figure 4a), which is mainly caused by less cooling due to solar CRE (Figure 4b), while the modeled terrestrial CRE again matches the observed surface terrestrial CRE (Figure 4c). The way ~~how~~ that the surface solar CRE is defined allows us to narrow down ~~,~~ which effect is the main cause for the overestimated net solar surface irradiances. If clouds ~~would be~~ were perfectly simulated by the model, the negatively biased surface albedo would cause a too strongly negative surface solar CRE. As this is not the case for ICON, it is inferred that the main ~~cause~~ reason for the overestimated net solar surface irradiances is related to overestimated transmissivity of the cloud layer, which is defined as the ~~fraction~~ ratio of downward transmitted solar irradiance at cloud base to downward incident solar irradiance at cloud top. Therefore, underestimated cooling effects in the solar spectral range are most likely related to incorrect simulations of microphysical or macrophysical properties of Arctic clouds in ICON. In the following section, we therefore compare those properties as they were simulated (ICON) and measured (ACLOUD) in more detail.

4 Comparison of macro- and microphysical cloud properties in ICON to ACLOUD observations

Transmissivity T of a cloud layer is directly related to its optical thickness τ_c:

$$T = \exp(-\tau_\mathrm{c}), \tag{1}$$

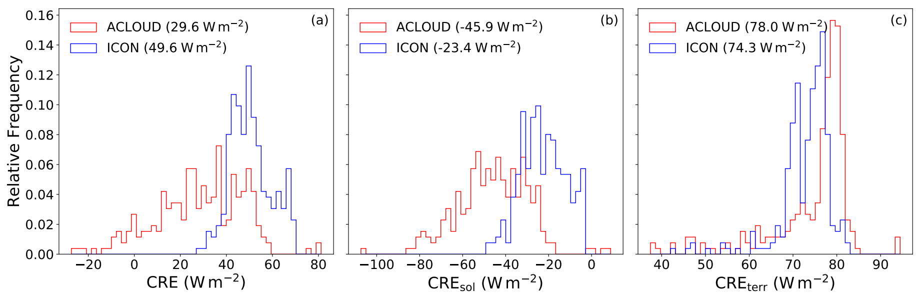

Figure 4. As Figure 3, but for the (a) total, (b) solar, and (c) terrestrial net cloud radiative effect at the surface.

where τ_c is defined as the ~~vertical integral of the volumetric cloud~~ volumetric cloud particle extinction coefficient β_{ext}, vertically integrated from cloud base z_{base} to cloud top z_{top}:

$$\tau_c = \int_{z_{base}}^{z_{top}} \beta_{ext}(z)\,dz. \quad (2)$$

During ACLOUD and PASCAL, clouds were mostly in the liquid water phase with only little ice present, which allows to express the extinction coefficient as a function of liquid water content q_c and cloud droplet number concentration N_d (Grosvenor et al., 2018):

$$\beta_{ext} \sim N_d^{\frac{1}{3}} \cdot q_c^{\frac{2}{3}}\,. \quad (3)$$

Equation 3 and Equation 2 show that τ_c depends on ~~macrophysical (geometrical depth ,~~ geometrical depth ($z_{top} - z_{base}$)~~and microphysical properties (i. e, N_d and~~ , as well as on q_c and N_d. In this study, we will denote the geometrical depth as a cloud macrophysical property and denote q_c ~~) of the cloud layer~~and N_d as cloud microphysical properties. Nevertheless, we are aware that liquid water content, especially in a model that employs a saturation adjustment, cannot be considered to be solely a microphysical property as it strongly depends on the thermodynamical state of the atmosphere, thus making it a macrophysical variable that is adjusted by microphysical processes.

To identify potential sources explaining the model-measurement differences discussed in the previous section, we compare geometrical cloud thickness and microphysical properties of clouds in ICON to observations collected during ACLOUD/PASCAL. We decided to focus on the period from 2 June to 5 June 2017, when flights were possible on three out of four days. ~~This period is favored because only low-level, mostly single layer clouds were present, which simplifies interpretation~~Here, only a brief summary of the meteorological conditions during that period is given. For a comprehensive overview of this period, we would refer the reader to Knudsen et al. (2018) and Wendisch et al. (2019). During this period, a southerly to easterly inflow of warm and moist air into the region where research flights took place was observed~~(Knudsen et al., 2018)~~. Average near-surface temperatures and integrated water vapor at R/V Polarstern during that period were -3° C and 6 kg m^{-2}, respectively. A relatively shallow, inversion-capped atmospheric boundary layer (Knudsen et al., 2018) with cloud top heights of less than 500 m in the vicinity of R/V Polarstern was observed. During those four days, the low-level cloud field was relatively homogeneous and mostly stratiform, with almost no high clouds being present in the domain where the research flights took place. Mostly liquid water and mixed-phase clouds were observed during this period (Wendisch et al., 2019). The relatively stable meteorological conditions during this period facilitated the statistical aggregation of the measurements all the research flights that took place during that period, which was not as straightforward for other parts of the campaign. Especially during mid June 2017, broken multi-layer clouds were present, which made a consistent comparison between the model and the observations harder to achieve. This can be seen in the limited amount of simultaneously cloudy and sea-ice-covered scenes in the period from 16 June to 18 June (see Table 1). Additionally, in-situ observation of cloud microphysical properties were performed on all flight days during that period. Another important point why this period was chosen is the fact R/V Polarstern was within the sea-ice-covered region and provided another source of observations that we can use for the comparison with our ICON simulations.

4.1 Geometrical cloud depth

We compare geometrical cloud depth as simulated by ICON to that observed during PASCAL. We choose PASCAL cloud radar and ceilometer observations instead of ACLOUD observations as they provide a continuous dataset in time, which facilitates the comparison of geometrical cloud depth. To better compare the simulations to ground based observations, we use ICON's meteogram output. It provides profiles of model variables at a certain location at every model timestep compared to the 30 minute output frequency when outputting the whole model domain. For each day simulated, we choose to output the profiles at Polarstern's 12 UTC location. While its position was rather constant from 3 June onward (Wendisch et al., 2019, their Figure 2), the ship was still in transit to the ice floe on 2 June. This might introduce some inconsistencies in the comparison to the spatially fixed ICON profiles. As the ship was already relatively far into the marginal sea ice zone, the cloud field should be homogeneous and representative for sea ice covered conditions.

For the model output, a layer within a profile is considered cloud covered if the the total cloud condensate (liquid and ice) is larger than a threshold of 0.05 g m^{-3}. We only assess clouds close to the surface, namely from the ground to 2 km altitude. In this altitude range, we define cloud base/top as the lowest/highest model level a cloud is being simulated within a profile. To derive the observed geometrical cloud depth, we use cloud base height as observed by the laser ceilometer on board R/V Polarstern while cloud top height was derived using the 35 GHz cloud radar (Griesche et al., 2019). Both modeled and observed cloud depths have been temporally interpolated to be on identical timesteps. We acknowledge that such a comparison of geometrical cloud thickness is not a definition aware comparison as it depends on instrument sensitivities and on the chosen threshold of total cloud condensate for diagnosing clouds in the model. Additionally, the rather simple approach is not able to correctly diagnose cloud depth for multi-layer clouds but as stated above, mostly single layer clouds were observed and simulated during the period of interest.

The comparison of difference in geometrical cloud depth for simulated by ICON and as observed from R/V Polarstern during the period from 2 June to 5 June is shown in Figure 5. In general, the geometrical cloud depth in ICON is in fair agreement with the observed geometrical cloud depth even though it shows a slight underestimation is slightly negatively biased in our ICON simulations with a mean bias of 65 m and a standard deviation of 110 m. In offline radiative transfer simulations, we explored

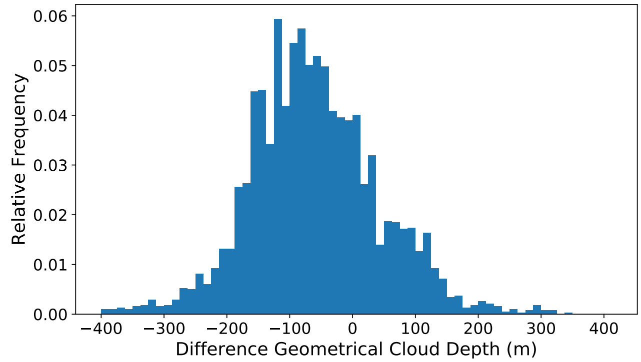

Figure 5. ~~Geometrical~~ Difference in geometrical cloud depth ~~as simulated by~~ between ICON and as observed from R/V Polarstern during the period from 2 June to 5 June.

the effect of this bias in cloud geometrical thickness on the solar component of the surface CRE (see supplement). For that, we used profiles of liquid water that have been observed during the period from 2 June to 5 June and interpolated those profiles in the vertical. For all those profiles, a bias in 65 m in cloud vertical extent lead to change in solar CRE of approximately 5 W m^{-2}, which is not sufficient to explain the reported model bias of more than 20 W m^{-2}. Therefore, we will now focus on how cloud microphysical properties are represented in ICON compared to the observations ~~. This can be a factor that to some extend contributes to the underestimated cloud optical thickness~~and to which extent they contribute to the ascertained biases in cloud optical properties.

4.2 Cloud microphysical properties

To investigate how cloud microphysical properties contribute to the underestimated cloud optical thickness in ICON, we make use of the suite of in situ instruments that were part of the instrumentation of Polar 6 (Ehrlich et al., 2019). From 2 June to 5 June, research flights with Polar 6 were performed on three out of four days (no flight on 3 June). We focus on particle size distribution of hydrometeors and the respective moments, which have been observed by the Small Ice Detector Mark 3 (SID-3) covering a size range of cloud droplets/ice crystals, from 5 to 40 μm. As particle size distributions derived from SID-3 agree well with those from other sensors (such as the Cloud Droplet Probe, CDP) for days when both probes were available (Ehrlich et al., 2019), we are confident that particle size distributions from the SID-3 are best suited for our comparison. In the following, we compare simulated and observed particle size distributions as well as the total ~~(droplets plus ice crystals)~~ particle number concentration (N_d)~~and~~ , mainly consisting of droplets in the size range presented in Figure 6. Furthermore, the liquid water content (q_c) is shown. To be comparable to the particle size distribution from the SID-3, we integrate the size distribution of the two-moment microphysical scheme implemented in ICON within the size bins of the SID-3 for cloud droplets and ice crystals, and add them. Due to relatively warm temperatures in the region of the research flights in early June 2017, only little ice was present in clouds during that period. While we derive the particle number concentration directly from particle size distribution by integrating over the size bins of the SID-3, we use measurements from the Nevzorov probe on Polar 6 to ~~get~~

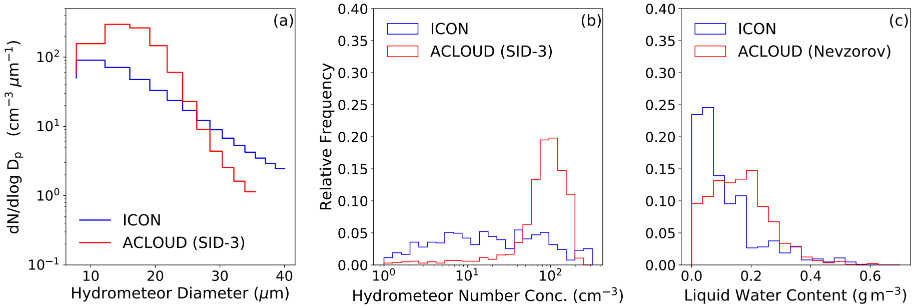

Figure 6. Time-space average particle number size distribution (a) and relative frequency of total particle number in the diameter range from 5 to 40 μm (b), as well as liquid water content (c). All data is averaged over the flights from 2 June to 5 June over sea ice covered region. Filtering for sea ice covered ACLOUD flight sections is done using simulated albedo from ICON.

obtain information on q_c.

Figure 6 shows particle number size distributions and the particle number concentration and liquid water content (~~LWC~~q_c) for the period from 2 June to 5 June. Looking at the particle size distributions, we find that ICON underestimates the number concentration for hydrometeors smaller than 25 μm, while it overestimates the amount of cloud particles larger than that threshold in comparison to the measurements. As the number concentration of hydrometeors is mainly influenced by the number of small particles, the total amount of hydrometeors is also underestimated in the model. Averaged over all bins, ~~the LWC~~ q_c is underestimated by ICON relative to ~~the LWC~~ q_c derived by the Nevzorov probe, as the models overestimates the frequency of occurrence for relatively small ~~LWC~~ q_c values.

5 Discussion

5.1 Representation of cloud microphysical parameters in ICON

According to Equation 3, the underestimated hydrometeor number concentration and ~~LWC~~ q_c both can lead to lower cloud optical thickness in ICON. As not all microphysical schemes in ICON do provide number concentration of cloud droplets and ice crystals, the calculation of cloud optical properties is simplified in the radiation scheme. As an input for the radiation routines for liquid water clouds in ICON, a constant profile of ~~cloud droplet number concentration (CDNC)~~ N_d is used, that decreases exponentially with altitude, and ~~LWC~~ q_c for the calculation optical properties of liquid clouds. For open water/sea ice, the assumed surface ~~CDNC~~ N_d within the radiation scheme is 80 cm^{-3}, which is close to the observed cloud hydrometeor number concentrations (Figure 6). Nevertheless, this value is slightly lower than ~~observed the~~ the observed mean of 85 cm^{-3} for the three flight days from 2 June to 5 June. Assuming that the model is able to correctly simulate ~~the LWC~~q_c, this underestimation would imply lower cloud optical thickness, which would further contribute to the overestimated amount of downward solar irradiance that reaches the surface. Calculation of optical properties of ice clouds is even further simplified as they ~~are solely depend~~ depend solely on the ice water content. To evaluate the effect of cloud ice on radiative properties in the model, we performed a sensitivity analysis in which we turned off any radiative effect of cloud ice. This analysis revealed only a minor impact of cloud ice on radiation properties like surface CRE and net irradiance at the surface, which was both on the order of $1\,\mathrm{W\,m^{-2}}$ compared to the basic set-up. This low impact is due to the already low cloud ice fraction in the model, which causes the radiative effect of cloud ice to be low. Due to the limitations of the observational dataset with little cloud ice being observed, it is hard to constrain the model from the observational side. Therefore, any estimation of the impact of cloud ice on the radiative balance has to be interpreted with some caution.

Additionally, ~~the LWC~~ q_c in the model is underestimated compared to the observations, which also contributes to the bias in cloud optical thickness in ICON. We attribute the lower ~~LWC~~ q_c to an underestimated number concentration of relatively small cloud droplets (diameters $< 25\,\mu$m), which are commonly observed for this region and season (Mioche et al., 2017). The model also overestimates the number of hydrometeors with diameters larger than 25 μm. Thus, too few cloud droplets are generated and, therefore, condensational growth and coalescence of the available cloud droplets shifts the size distribution towards larger droplets. Looking at the phase state of precipitation reaching the surface ~~(not shown),~~ in the region around R/V Polarstern (81°-85° N and 5°-15° E), where most of the research flights from 2 June to 5 June took place, we find that ~~the amount of rain is~~ rain rate at the surface ($8.57\,\mathrm{g\,m^{-2}\,h^{-1}}$) is almost an order of magnitude large than ~~the amount of snow~~ that of snow ($2.95\,\mathrm{g\,m^{-2}\,h^{-1}}$). As temperatures in the atmospheric boundary layer over sea ice were mostly below freezing during the three days analyzed, this ~~precipitation must stems~~ rain must stem from "warm" rain processes, indicating an relatively active autoconversion process in our set-up. Therefore, autoconversion further contributes to the underestimated ~~LWC~~ q_c by ICON as it acts ~~for a sink of~~ as a sink for cloud liquid water.

Interestingly, the here reported systematic underestimation of hydrometeors is different from the findings by Schemann and Ebell (2020). They conducted simulations for the Ny-Ålesund research station using the ICON model in the large-eddy set-up (ICON-LEM), and compare ground-based cloud radar observations with their ICON-LEM simulations applying a radar forward operator. Besides a different scheme for turbulent transport and activated parameterization of shallow convection in our set-up, as well as corresponding initial/boundary conditions from DWD's operational ICON forecast (instead of ECMWF forecast), the basic set-up is similar to our simulations. Comparing radar reflectivities using contoured frequency by altitude diagrams in mid June 2017 (see Figure 6 in Schemann and Ebell, 2020), they found that for their 75 m domain, the model strongly overestimates the frequency of occurrence for low radar reflectivities/small hydrometeors. They argue that this finding can be related to the way CCN ~~get~~ are activated into cloud droplets in the default Seifert-Beheng two-moment microphysical scheme. This was confirmed by ICON-LEM simulations in an Arctic domain by Mech et al. (2020) who implemented different CCN activation scheme (Phillips et al., 2008) within the Seifert-Beheng two-moment microphysics.

5.2 Revised activation of CCN in ICON

In the following, we will focus on the issue of the non-matching particle number size distribution compared to ACLOUD observations and how it affects total droplet number and ~~LWC~~ q_c of clouds in our simulations. As it has been pointed out by Schemann and Ebell (2020), this process might presently be misrepresented in the model. In its present implementation into ICON, the activation of CCN is parameterized as a function of grid-scale vertical velocity $\overline{w}$ and pressure p as described in

Hande et al. (2016):

$$\text{CCN}_{\text{act}} = A(p) \cdot \arctan\left[B(p) \cdot \log(\overline{w}) + C(p)\right] + D(p)\,, \tag{4}$$

where the parameters $A(p)$ to $D(p)$ contain information on the vertical profile of CCN and on the activation of CCN with respect to grid-scale vertical velocity $\overline{w}$. The profile presently used in the two-moment microphysical scheme is a temporally and spatially constant profile taken over Germany for a day in April 2013 as in Heinze et al. (2017). This CCN activation profile is not representative for the amount of CCN in the Arctic domain, as the CCN concentration in the Arctic is much lower. As stated in Schemann and Ebell (2020), the overestimated frequency of occurrence for low radar reflectivities/small hydrometeors in their simulations can be related to this unsuitable CCN profile.

~~It~~ Despite this unsuited CCN activation profile for an Arctic domain, we find an underestimated amount of hydrometeors in our simulations. Therefore, it is plausible that the relatively low hydrometeor number concentration is related to the coarser resolution in our ICON simulations. A realistic simulation of turbulence and cloud-scale vertical motion is crucial for Arctic mixed-phase clouds (Rauber and Tokay, 1991; Korolev and Field, 2008; Shupe et al., 2008). As the number of activated CCN is a function of grid-scale vertical velocity, it is likely that our simulations at 1.2 km resolution do not sufficiently resolve in-cloud vertical motion and turbulence (Tonttila et al., 2011). This is consistent with the fact that characteristic eddy ~~size~~ sizes in Arctic mixed-phase clouds is less than 1 km (Pinto, 1998). Fan et al. (2011) suggested that only horizontal model resolutions of less than 100 m are able to resolve major dynamic features that contribute to vertical motion in Arctic mixed-phase clouds. Not being able to resolve those features consequently affects particle size distributions and its moments like number concentration as too few droplets are activated (Morrison and Pinto, 2005).

To account for subgrid-scale vertical motion, vertical velocity in the aerosol activation in larger scale models is often parameterized as a function of specific turbulent kinetic energy (Ghan et al., 1997; Lohmann et al., 1999), TKE, which is defined as:

$$\text{TKE} = \frac{1}{2} \cdot \overline{(u'^2 + v'^2 + w'^2)}\,, \tag{5}$$

where the u', v', w' are the subgrid-scale deviations from grid-scale velocitiy and the overbar denotes grid-box average. To explore the effects of including sub-grid scale vertical velocity in the Hande et al. (2016) CCN activation parametrization, we choose to follow a similar approach as proposed in Ghan et al. (1997), who assume the sub-grid vertical velocity in a grid box to follow a Gaussian distribution $P(w\,|\,\overline{w}, {\sigma_w}^2)$. The grid box averaged number of activated CCN can, therefore, be written as the integral over positive vertical velocities:

$$\overline{\text{CCN}_{\text{act}}} = \int_0^{\infty} P(w\,|\,\overline{w}, {\sigma_w}^2) \cdot \text{CCN}_{\text{act}}(w)\,\mathrm{d}w\,. \tag{6}$$

To numerically solve the integral in Equation 6, a ~~relatively~~ simple trapezoidal integration is employed using 50 equally spaced bins in a $\pm 3\,\sigma_w$ range around $\overline{w}$.

If it is assumed that sub-grid scale motion in low-level Arctic mixed-phase clouds is isotropic ($u'^2 = v'^2 = w'^2$), as proposed

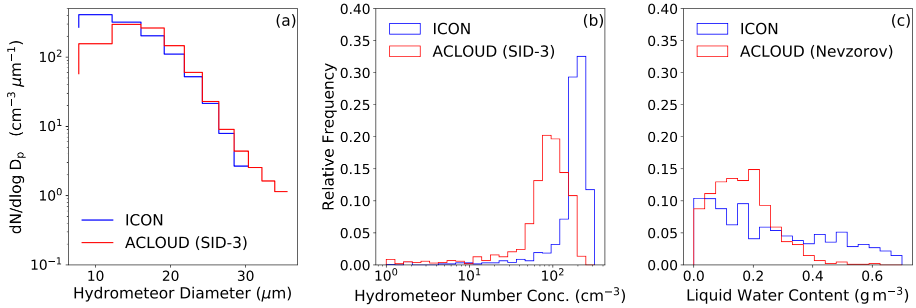

Figure 7. As Figure 6 but for the revised CCN activation. ~~All~~ Due to different cloud fields in this simulation, the red lines (ACLOUD) are not identical ~~to~~ with Figure 6 because of the ~~corresponding red lines~~ sampling strategy employed as only datapoints in the observations and the simulation are being used if both are within a cloud simultaneously.

by Pinto (1998), the variance of vertical velocity can be expressed as function of TKE as follows (Morrison and Pinto, 2005):

$$\sigma_w{}^2 = w'^2 = \frac{2}{3} \cdot \mathrm{TKE}\,. \tag{7}$$

Using turbulence measurements on a tethered balloon during the PASCAL ice floe operations, Egerer et al. (2019) showed that isotropic turbulence is a valid assumption for a subset of days during PASCAL that have been analyzed in their study. We, nevertheless, are aware that isotropic sub-grid scale motion in Arctic clouds cannot be assumed for all conditions (Curry et al., 1988; Finger and Wendling, 1990).

The effects of this revised CCN activation for the period from 2 June to 5 June are shown in Figure 7. Compared to the original activation parameterization, the model shows a much closer agreement with the measurements, although an overestimation of hydrometeors with diameters less than 20 μm is simulated, while it underestimates the number of hydrometeors larger than 30 μm. As the number of small hydrometeors governs the total number of hydrometeors, their overestimation ~~now also~~ leads to an overestimated number of total hydrometeors in the whole diameter range between 5 and 40 μm. The particle size distribution now is in better agreement with the findings by Schemann and Ebell (2020), as we find an overestimation of smaller hydrometeors and underestimated number concentration of larger hydrometeors compared to in situ observations. The shift of the particle size distribution towards smaller hydrometeors can be related to the unsuited CCN profile within the activation parameterization. ~~The increased number of hydrometeors also affects the LWC, which is more evenly distributed over the mass density bins, ranging up to 0.6 g m^{-3}~~As discussed above, autoconversion is the predominant sink for cloud water in the absence of precipitation formation via the ice phase. The fact that the revised activation of CCN increases N_d eventually leads to a reduction in the size of cloud droplets (see Figure 7a). This reduces the collection efficiency of cloud droplets which leads to a less efficient autoconversion process, which can be seen in the shift in the histogram of q_c towards higher values in Figure 7c. Compared to the ACLOUD observations, small values of liquid water content less then 0.3 g m^{-3} are underestimated, while values larger than that threshold are simulated more frequently in the revised CCN activation.

The presently used CCN activation profile was originally derived for spring conditions in Germany, where one would expect a much higher load of CCN compared to the Arctic. To have a more realistic representation of CCN, a dedicated simulation

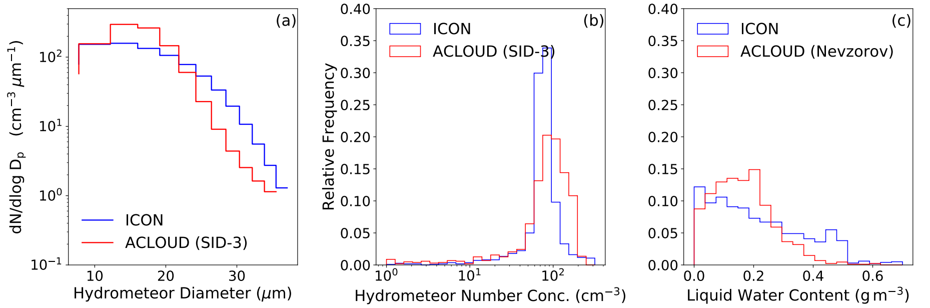

Figure 8. As Figure 7 but with scaled number of activated CCN by a factor of 0.4. ~~All~~ Due to different cloud fields in this simulation, the red lines (ACLOUD) are not identical ~~to~~ with Figure 6 and Figure 7 because of the ~~corresponding red lines~~ sampling strategy employed as only datapoints in the observations and the simulation are being used if both are within a cloud simultaneously.

with a model that is able to represent the formation and transport of aerosols would be necessary. We opt against this approach and ~~just~~ instead scale the number of activated CCN from the default profile using a scaling factor of 0.4. A more elaborate description why this scaling factor was used is given in Appendix A. The chosen scaling factor ~~now~~ results in an underestimated number of hydrometeors smaller than 22 μm as it is shown in Figure 8, while hydrometeors with larger diameters are overestimated by the model. Looking at the hydrometeors number concentration, the chosen scaling factor shifts the simulated distribution towards smaller hydrometeor concentrations that consequently results in a slight underestimation of hydrometeors compared to the observations. This indicates that the chosen scaling factor is slightly too effective in reducing the number of activated CCN. Compared to Figure 7, high values of liquid water content larger than 0.3 g m^{-3} occur less frequently when scaling the number of activated CCN, but there is still a slight underestimation in the frequency of occurrence for ~~LWC~~ q_c values between 0.1 g m^{-3} and 0.3 g m^{-3}. Even though scaled, the overall shape of the profile of activated CCN as a function of vertical velocity remains unchanged. A different aerosol composition or just a different vertical profile of aerosols alter the shape of the profile, which might also lead to biases in the number of activated CCN. This emphasizes the need for an CCN activation profile that is better suited for an Arctic environment, which has also been proposed by Schemann and Ebell (2020).

The effect of the different CCN activation set-ups on the CRE for all flights from 2 June to 5 June is shown in Figure 9 (a)-(c). We would like to point out that the cloud fields between the respective CCN activation set-ups vary. For that reason, the number of available datapoints for which the threshold for sea ice coverage and cloudy conditions are fulfilled at the same time, differ between the runs due to the filtering that is employed. Similar to the histograms in Figure 4, which cover all flights used in this comparison, the warming effect of clouds at the surface is overestimated when looking at the period from 2 June to 5 June. For the revised CCN activation, the increase in ~~LWC~~ q_c reflects on the surface CRE, which now has a small negative bias compared to the ACLOUD observations. Because of the aforementioned constant profile of cloud droplet number concentrations in the calculation of the effective radius within the radiation scheme, this negative bias would be more strongly expressed if the actual cloud droplet number concentration from the microphysical scheme would be used (see subsection 5.3). When scaling the activated number of CCN by a factor of 0.4 using the revised CCN activation, the CRE is still overestimated by ICON compared to observations even though the positive bias in the median could be reduced by approximately 5 W m^{-1}. As downscaling the number of activated CCN by a factor of 0.4 was already slightly too effective in reducing the hydrometeor number, a larger scaling factor might be able to further decrease the CRE in the model.

From the previously conducted sensitivity study employing a more effective CCN activation, it is not clear whether the above reported biases in cloud microphysical properties is a source (inefficient CCN activation) or a sink issue (too effective autoconversion). To this end, we conducted a further sensitivity study with unchanged CCN profile and in which autoconversion was turned off entirely (see supplement). While the effect on q_c is comparable to the revised, but not yet scaled CCN activation (see Figure 7), the cloud droplet number concentration is still underestimated. Furthermore, the shape of the size distribution does not match the shape of the observed one. Since the CCN profile used in the activation of CCN into cloud droplets within the cloud microphysical scheme is not suited for an Arctic domain as it overestimates the availability of CCN, the underestimated amount of cloud droplets in the simulations with autoconversion turned off is indicative for a source rather then a sink problem of cloud droplets in our simulations.

5.3 Coupling of hydrometeor number concentration to radiation

As already discussed above, there is an inconsistency between the hydrometeor number concentration derived in the two-moment microphysics and used in the radiation routines. In the following, we therefore explore the effect of making the hydrometeor concentrations consistent between the two parametrizations. As input for the calculation of optical properties, ICON uses cloud droplet/ice crystal effective radius, which is defined as the ratio of the third to the second moment of the size distribution. Previously, effective radii were computed as a function solely of specific masses.

To ensure consistency with the size distributions in the Seifert-Beheng two-moment scheme, we calculate the effective radii from the used gamma distribution (see Appendix B for the derivation). This new implementation has already been used in Costa-Surós et al. (2020). In Figure 9 (d)-(f), the biggest difference to the uncoupled hydrometeor number concentrations (Figure 9 (a)-(c)) can be seen in the histograms for the revised CCN activation (Figure 9 (e)). In this set-up, the CRE is underestimated compared to observations due to higher hydrometeor concentration, which is now also considered in the radiation parameterization. For the revised and scaled CCN activation, only little differences are simulated between coupled and uncoupled hydrometeor concentration. As stated above, the fixed cloud droplet number concentration in the default radiation routines is already relatively close to the hydrometeor concentration observed for the flights from 2 June to 5 June. Nevertheless, compared to the observations, the median value of the CRE in ICON in Figure 9 (ef) is closest to the observed values, even though they are still slightly overestimated. Altogether, the revised CCN activation with a scaled CCN activation and coupled hydrometeor now results in a positive bias of only approximately 6 W m^{-2}. The effect on surface CRE of the coupling of hydrometeor number concentration to radiation for this period is relatively low (1 W m^{-2}, see Figure 9 (c) and (ef)), as the assumed number concentration in the default set up and the number concentrations from two-moment microphysical scheme in the revised and scaled CCN activation are in a similar range. As can be seen from Figure 9 (b) and (e), if the CDNC N_d profile in the microphysics deviates from the profile in the radiation, there can be quiet substantial differences due to a more

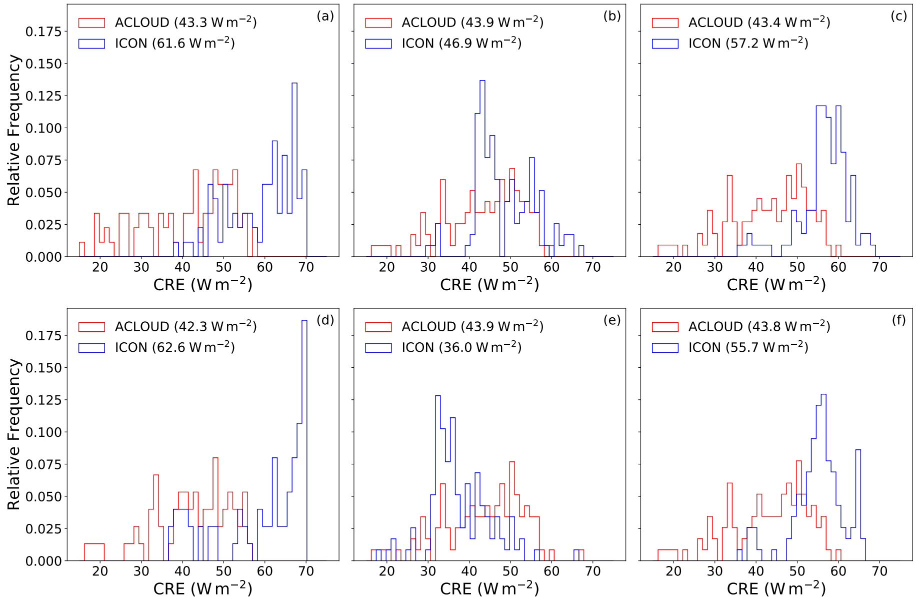

Figure 9. As Fig. 4a, but for the flights from 2 June to 5 June only, for the default set-up (a), for the revised CCN activation (b) and for the revised CCN activation with scaled number of activated CCN by a factor of 0.4 (c). The bottom row (d-f) as the top row but with hydrometeor number concentration coupled to radiation. Due to different cloud fields in the respective simulations, the histograms for the ACLOUD observations are not identical as only datapoints in the observations and the simulation are being used if both are within a cloud simultaneously.

realistic representation of the Twomey effect (Twomey, 1977), which can be important for relatively clean/polluted situations. As it can be seen in Figure 4, the differences in the CRE for the respective sensitivity experiments are again primarily mediated by its solar component, whereas the terrestrial components are in good agreement with the observationally derived terrestrial CRE components (see supplement).

6 Conclusions

In this study, we use observational data from the ACLOUD and PASCAL campaigns (Wendisch et al., 2019) to compare it to limited-area simulations with the ICON atmospheric model at kilometer-scale resolution. While the model compares well to the observations in its ability to simulate the four cloud-surface radiation regimes in the Arctic, it severely underestimates cloud radiative effects in the solar ~~spectrum~~spectral range. This is despite a slight ~~overestimation~~ underestimation of the geometrical cloud thickness and attributable to too small droplet number concentrations and too little liquid water content simulated by the model. We showed that it is crucial to correctly ~~simulate~~ represent in-cloud turbulence in Arctic clouds, which is essential to correctly simulate hydrometeor number concentration and liquid water content. The findings of this study are mainly representative in the case of turbulence driven, stratiform and optically thin single-layer clouds that contain liquid water but are, to some extent, also valid for multi-layer clouds, which was confirmed by an analysis of days in mid June 2017, where such conditions prevailed. Furthermore, similar improvements were obtained at lower horizontal and vertical resolution (2.4 km and 50 vertical levels) when including sub-grid vertical motion in the activation of CCN into clouds droplets, which makes us confident that such an approach can also be beneficial for simulations with coarser spatial resolution.

As reported by Stevens et al. (2020), the representation of clouds in atmospheric models benefits from higher resolved simulation. Nevertheless, long time, global simulations at hectometer scale will not be feasible in the foreseeable future (Schneider et al., 2017), whereas climate projections at kilometer-scale can be achievable (Stevens et al., 2019). It is~~therefore~~, therefore, important to especially improve models on such scales to enable them to make realistic ~~simulation~~simulations. As shown in this study, aircraft observations are a valuable source of information and can be used for evaluating and improving the representation of physical processes for models at kilometer-scale. The results presented in our study might also be beneficial to the representation of clouds in ICON in other regions, where clouds are also turbulence-driven.

Data availability. The ICON model output data used in this study is stored at the German Climate Computing Center (DKRZ) and is available upon request from the corresponding author. The observational data from the ACLOUD/PASCAL campaigns archived on PANGAEA repository and can be accessed from the following DOIs: broadband (solar and terrestrial) irradiances (https://doi.org/10.1594/PANGAEA.902603, Stapf et al., 2019), Small Ice Detector Mark 3 (SID-3) (https://doi.org/10.1594/PANGAEA.900261, Schnaiter and Järvinen, 2019), Nevzorov probe (https://doi.org/10.1594/PANGAEA.906658, Chechin, 2019) and cloud radar 35 GHz cloud radar onboard of R/V Polarstern (https://doi.org/10.1594/PANGAEA.899895, Griesche et al., 2019).

Appendix A: Scaling of the default CCN profile

In this study, we decided to scale to default CCN profile in ICON to match values representative for the Arctic. The scaling factor is derived from aerosol mass mixing ratios from the re-analysis of atmospheric composition of the Copernicus Atmospheric Monitoring Service (CAMS; Inness et al., 2019), which assimilated MODerate Resolution Imaging Spectroradiometer (MODIS) aerosol retrievals (Levy et al., 2013) into the ECMWF model (Benedetti et al., 2009). We computed the number of activated CCN for various vertical velocities and also supersaturation for a sea ice covered domain north of Svalbard during the period from 2 June to 5 June following the approach of Block (2018). Close to the surface, the number of activated CCN at a supersaturation of 0.5 % in this dataset is approximately 45 cm^{-3}. This value is on the lower end of the observed number concentrations of activated CCN during PASCAL, which were in a range of 40 to 80 cm^{-3} during this period (Wendisch et al., 2019, their Figure 10).

To decide which scaling factor to use, we looked for a scaling factor (in steps of 0.05) that minimizes the mean squared error of the scaled profile and the profile derived from CAMS for several vertical velocities in an altitude band from the surface to 700 hPa. From Table A1, we find that a scaling factor of 0.4 is a good compromise for relatively low vertical velocities in Arctic clouds. Even though scaled to best match the CAMS profile, the overall shape of the profile of activated CCN in ICON remains unchanged. Figure A1 shows that the default profile strongly overestimates the number of activated CCN close to

Table A1. Scaling factor that minimizes the mean squared error of the scaled default activation profile in ICON and the activation profile derived from CAMS for several vertical velocities in an altitude band from the surface to 700 hPa.

w ($\mathrm{m\,s^{-1}}$)	0.01	0.03	0.08	0.22	0.60
Scaling factor	0.5	0.4	0.4	0.4	0.3

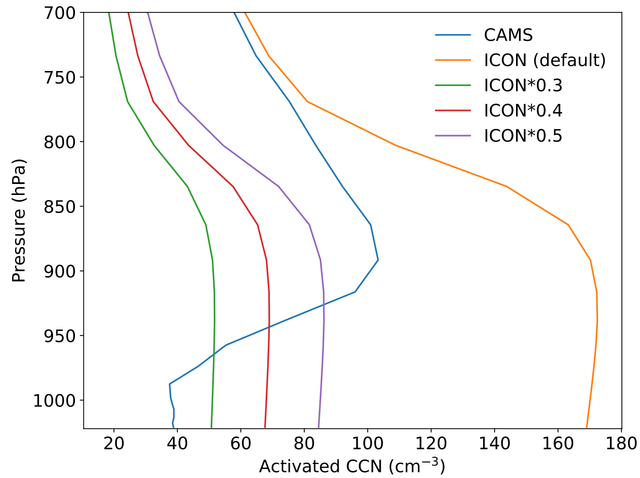

Figure A1. Profile of activated CCN at 0.08 $\mathrm{m\,s^{-1}}$ from CAMS and from the default profile in ICON. Additionally, a subset of scaled ICON profiles is shown.

the surface while nicely matches the CAMS profile for altitudes higher than 800 hPa. As almost all clouds from 2 June to 5 June were below that altitude, it is more important to correctly represent the number of activated aerosol close to the surface. The number of activated CCN is almost constant up to 850 hPa, whereas the number of activated CCN in the CAMS profile increases with altitude. Even though we cannot match the shape of the activation profile, a scaling factor of 0.4 should represent an approximate average up to 850 hPa.

Appendix B: Derivation of effective radius from gamma distribution

To describe the particle size distributions of all hydrometeor categories in the Seifert-Beheng two-moment microphysical scheme (Seifert and Beheng, 2006), a modified gamma distribution is used:

$$f(x) = A x^{\nu} \exp\left(-\lambda x^{\mu}\right), \tag{B1}$$

where x is the particle mass and ν and μ are the parameters of the distribution for the respective hydrometeor category. A and λ can be expressed by the number/mass densities and the parameters ν and μ (Eq. 80, Seifert and Beheng, 2006). Following

Petty and Huang (2011), the k-th moment M_k of such a modified gamma distribution can be expressed as follows:

$$M_k = \frac{A}{\mu} \frac{\Gamma\left(\frac{\nu+k+1}{\mu}\right)}{\lambda^{(\nu+k+1)/\mu}} . \tag{B2}$$

The ration between 3th and 2th moment can, therefore, be written as:

$$\frac{M_3}{M_2} = \frac{\Gamma\left(\frac{\nu+4}{\mu}\right)}{\Gamma\left(\frac{\nu+3}{\mu}\right)} \lambda^{\frac{-1}{\mu}} . \tag{B3}$$

To obtain the effective radius, Equation B1 has to be first converted into a function of radius. According to Eq. 54 in Petty and Huang (2011) the particle size distribution as a function of radius $f(r)$ can be written as:

$$A_r \, r^{\nu_r} \exp\left(-\lambda_r \, r^{\mu_r}\right) = A \, x(r)^{\nu} \exp\left[-\lambda \, r^{\mu}\right] \frac{\mathrm{d}x}{\mathrm{d}r} , \tag{B4}$$

The particle mass as a function of radius $x(r)$ in the Seifert-Beheng two-moment microphysical scheme is defined as follows:

$$x(r) = \left(\frac{2\,r}{a}\right)^{\frac{1}{b}} , \tag{B5}$$

which differs from the functional relationship given in Table 1 in Petty and Huang (2011), as the values for a and b are defined differently (see Table 1 in Seifert and Beheng, 2006). Therefore:

$$\frac{\mathrm{d}x}{\mathrm{d}r} = \left(\frac{2}{a}\right)^{\frac{1}{b}} \frac{1}{b} r^{\left(\frac{1}{b}-1\right)} . \tag{B6}$$

Inserting Equation B5 and Equation B6 into Equation B4 and comparing the respective parameters for radius and mass in Equation B1, we find the following conversion relationships for the parameters in the particle size distribution:

$$A_r = \frac{A}{b} \left(\frac{2}{a}\right)^{\frac{\nu+1}{b}} , \quad \nu_r = \frac{\nu + 1 - b}{b} , \quad \lambda_r = \lambda \left(\frac{2}{a}\right)^{\frac{\mu}{b}} , \quad \mu_r = \frac{\mu}{b} . \tag{B7}$$

By inserting those parameters into Equation B3 and applying the functional dependencies for A and λ from Eq. 80 in Seifert and Beheng (2006), the effective radius r_{eff} can be written as follows:

$$r_{\text{eff}} = \left[\frac{\Gamma\left(\frac{\nu+1}{\mu}\right)}{\Gamma\left(\frac{\nu+2}{\mu}\right)}\right]^{b} \left(\frac{q}{N}\right)^{b} \frac{a}{2} \frac{\Gamma\left(\frac{\nu+1+3b}{\mu}\right)}{\Gamma\left(\frac{\nu+1+2b}{\mu}\right)} , \tag{B8}$$

where q and N are the mass and number density for the respective hydrometeor category.

Author contributions. JK, JS, MW and JQ this conceived this study. DK helped setting up the input data for the ICON runs and gave valuable expertise on how to run the model in a limited area set-up. JK and JS prepared and analyzed the model and observational data, respectively. All of the authors assisted with the interpretation of the results. JK prepared the manuscript with contributions from all co-authors.

Competing interests. The authors declare that they have no conflict of interest.

Disclaimer. TEXT

Acknowledgements. We gratefully acknowledge the funding by the Deutsche Forschungsgemeinschaft (DFG, German Research Foundation) - 268020496 - TRR 172, within the Transregional Collaborative Research Center "ArctiC Amplification: Climate Relevant Atmospheric and SurfaCe Processes, and Feedback Mechanisms (AC)^3. The ICON model is jointly developed by German Weather Service (DWD) and the Max Planck Institute for Meteorology, Hamburg, and we thank the colleagues for making the model available to the research community. We furthermore thank the colleagues that participated in the ACLOUD/PASCAL campaigns for providing the datasets used in this study. Simulations were conducted at the German Climate Computing Center (Deutsches Klimarechenzentrum, DKRZ). We thank Axel Seifert ~~, Kerstin Ebell and Vera Schemann~~ and Kerstin Ebell for giving valuable comments on this manuscript. We furthermore thank the two anonymous reviewers for their constructive comments.

References

Baldauf, M., Seifert, A., Förstner, J., Majewski, D., Raschendorfer, M., and Reinhardt, T.: Operational Convective-Scale Numerical Weather Prediction with the COSMO Model: Description and Sensitivities, Monthly Weather Review, 139, 3887–3905, https://doi.org/10.1175/MWR-D-10-05013.1, 2011.

Barton, N. P., Klein, S. A., Boyle, J. S., and Zhang, Y. Y.: Arctic synoptic regimes: Comparing domain-wide Arctic cloud observations with CAM4 and CAM5 during similar dynamics, Journal of Geophysical Research Atmospheres, 117, https://doi.org/10.1029/2012JD017589, 2012.

Bechtold, P., Köhler, M., Jung, T., Doblas-Reyes, F., Leutbecher, M., Rodwell, M. J., Vitart, F., and Balsamo, G.: Advances in simulating atmospheric variability with the ECMWF model: From synoptic to decadal time-scales, Quarterly Journal of the Royal Meteorological Society, 134, 1337–1351, https://doi.org/10.1002/qj.289, 2008.

Benedetti, A., Morcrette, J.-J., Boucher, O., Dethof, A., Engelen, R. J., Fisher, M., Flentje, H., Huneeus, N., Jones, L., Kaiser, J. W., Kinne, S., Mangold, A., Razinger, M., Simmons, A. J., and Suttie, M.: Aerosol analysis and forecast in the European Centre for Medium-Range Weather Forecasts Integrated Forecast System: 2. Data assimilation, Journal of Geophysical Research, 114, D13 205, https://doi.org/10.1029/2008JD011115, 2009.

Bentley, J. L.: Multidimensional binary search trees used for associative searching, Communication Association for Computing Machinery, 18, 509–517, https://doi.org/10.1145/361002.361007, 1975.

Block, K.: Aerosol-Cloud-Radiation interactions in regimes of liquid water clouds, Phd thesis, University Leipzig, https://research.uni-leipzig.de/climate/block{_}karoline{_}{_}phd{_}{_}2018.pdf, 2018.

Block, K., Schneider, F. A., Mülmenstädt, J., Salzmann, M., and Quaas, J.: Climate models disagree on the sign of total radiative feedback in the Arctic, Tellus A: Dynamic Meteorology and Oceanography, 72, 1–14, https://doi.org/10.1080/16000870.2019.1696139, 2020.

Bodas-Salcedo, A., Webb, M. J., Bony, S., Chepfer, H., Dufresne, J.-L., Klein, S. A., Zhang, Y., Marchand, R., Haynes, J. M., Pincus, R., and John, V. O.: COSP: Satellite simulation software for model assessment, Bulletin of the American Meteorological Society, 92, 1023–1043, https://doi.org/10.1175/2011BAMS2856.1, 2011.

Boeke, R. C. and Taylor, P. C.: Evaluation of the Arctic surface radiation budget in CMIP5 models, Journal of Geophysical Research: Atmospheres, 121, 8525–8548, https://doi.org/10.1002/2016JD025099, 2016.

Cesana, G., Kay, J. E., Chepfer, H., English, J. M., and De Boer, G.: Ubiquitous low-level liquid-containing Arctic clouds: New observations and climate model constraints from CALIPSO-GOCCP, Geophysical Research Letters, 39, https://doi.org/10.1029/2012GL053385, 2012.

Chechin, D.: Liquid water content measured by the Nevzorov probe during the aircraft ACLOUD campaign in the Arctic, https://doi.org/10.1594/PANGAEA.906658, 2019.

Costa-Surós, M., Sourdeval, O., Acquistapace, C., Baars, H., Carbajal Henken, C., Genz, C., Hesemann, J., Jimenez, C., König, M., Kretzschmar, J., Madenach, N., Meyer, C. I., Schrödner, R., Seifert, P., Senf, F., Brueck, M., Cioni, G., Engels, J. F., Fieg, K., Gorges, K., Heinze, R., Siligam, P. K., Burkhardt, U., Crewell, S., Hoose, C., Seifert, A., Tegen, I., and Quaas, J.: Detection and attribution of aerosol–cloud interactions in large-domain large-eddy simulations with the ICOsahedral Non-hydrostatic model, Atmospheric Chemistry and Physics, 20, 5657–5678, https://doi.org/10.5194/acp-20-5657-2020, 2020.

Curry, J. A., Ebert, E. E., and Herman, G. F.: Mean and turbulence structure of the summertime Arctic cloudy boundary layer, Quarterly Journal of the Royal Meteorological Society, 114, 715–746, https://doi.org/10.1002/qj.49711448109, 1988.

Dipankar, A., Stevens, B., Heinze, R., Moseley, C., Zängl, G., Giorgetta, M., and Brdar, S.: Large eddy simulation using the general circulation model ICON, Journal of Advances in Modeling Earth Systems, 7, 963–986, https://doi.org/10.1002/2015MS000431, 2015.

Egerer, U., Gottschalk, M., Siebert, H., Ehrlich, A., and Wendisch, M.: The new BELUGA setup for collocated turbulence and radiation measurements using a tethered balloon: First applications in the cloudy Arctic boundary layer, Atmospheric Measurement Techniques, 12, 4019–4038, https://doi.org/10.5194/amt-12-4019-2019, 2019.

Ehrlich, A., Wendisch, M., Lüpkes, C., Buschmann, M., Bozem, H., Chechin, D., Clemen, H.-C., Dupuy, R., Eppers, O., Hartmann, J., Herber, A., Jäkel, E., Järvinen, E., Jourdan, O., Kästner, U., Kliesch, L.-L., Köllner, F., Mech, M., Mertes, S., Neuber, R., Ruiz-Donoso, E., Schnaiter, M., Schneider, J., Stapf, J., and Zanatta, M.: A comprehensive in situ and remote sensing data set from the Arctic CLoud Observations Using airborne measurements during polar Day (ACLOUD) campaign, Earth System Science Data, 11, 1853–1881, https://doi.org/10.5194/essd-11-1853-2019, 2019.

Eirund, G. K., Possner, A., and Lohmann, U.: Response of Arctic mixed-phase clouds to aerosol perturbations under different surface forcings, Atmospheric Chemistry and Physics, 19, 9847–9864, https://doi.org/10.5194/acp-19-9847-2019, 2019.

Emde, C., Buras-Schnell, R., Kylling, A., Mayer, B., Gasteiger, J., Hamann, U., Kylling, J., Richter, B., Pause, C., Dowling, T., and Bugliaro, L.: The libRadtran software package for radiative transfer calculations (version 2.0.1), Geoscientific Model Development, 9, 1647–1672, https://doi.org/10.5194/gmd-9-1647-2016, 2016.

English, J. M., Gettelman, A., and Henderson, G. R.: Arctic Radiative Fluxes: Present-Day Biases and Future Projections in CMIP5 Models, Journal of Climate, 28, 6019–6038, https://doi.org/10.1175/JCLI-D-14-00801.1, 2015.

Fan, J., Ghan, S., Ovchinnikov, M., Liu, X., Rasch, P. J., and Korolev, A.: Representation of Arctic mixed-phase clouds and the Wegener-Bergeron-Findeisen process in climate models: Perspectives from a cloud-resolving study, Journal of Geophysical Research, 116, D00T07, https://doi.org/10.1029/2010JD015375, 2011.

Finger, J. E. and Wendling, P.: Turbulence Structure of Arctic Stratus Clouds Derived from Measurements and Calculations, Journal of the Atmospheric Sciences, 47, 1351–1373, https://doi.org/10.1175/1520-0469(1990)047<1351:TSOASC>2.0.CO;2, 1990.

Flores, H. and Macke, A.: The Expeditions PS106/1 and 2 of the Research Vessel POLARSTERN to the Arctic Ocean in 2017, Berichte zur Polar- und Meeresforschung, 714, https://doi.org/10.2312/BzPM_0714_2017, https://doi.org/10.2312/BzPM{_}0714{_}2017, 2018.

Fridlind, A. M., Ackerman, A. S., McFarquhar, G., Zhang, G., Poellot, M. R., DeMott, P. J., Prenni, A. J., and Heymsfield, A. J.: Ice properties of single-layer stratocumulus during the Mixed-Phase Arctic Cloud Experiment: 2. Model results, Journal of Geophysical Research Atmospheres, 112, 1–25, https://doi.org/10.1029/2007JD008646, 2007.

Gasteiger, J., Emde, C., Mayer, B., Buras, R., Buehler, S., and Lemke, O.: Representative wavelengths absorption parameterization applied to satellite channels and spectral bands, Journal of Quantitative Spectroscopy and Radiative Transfer, 148, 99–115, https://doi.org/10.1016/j.jqsrt.2014.06.024, 2014.

Ghan, S. J., Leung, L. R., Easter, R. C., and Abdul-Razzak, H.: Prediction of cloud droplet number in a general circulation model, Journal of Geophysical Research: Atmospheres, 102, 21 777–21 794, https://doi.org/10.1029/97JD01810, 1997.

Giorgetta, M. A., Brokopf, R., Crueger, T., Esch, M., Fiedler, S., Helmert, J., Hohenegger, C., Kornblueh, L., Köhler, M., Manzini, E., Mauritsen, T., Nam, C., Raddatz, T., Rast, S., Reinert, D., Sakradzija, M., Schmidt, H., Schneck, R., Schnur, R., Silvers, L., Wan, H., Zängl, G., and Stevens, B.: ICON-A, the Atmosphere Component of the ICON Earth System Model: I. Model Description, Journal of Advances in Modeling Earth Systems, 10, 1613–1637, https://doi.org/10.1029/2017MS001242, 2018.

Griesche, H., Seifert, P., Engelmann, R., Radenz, M., and Bühl, J.: OCEANET Cloud radar Mira-35 during POLARSTERN cruise PS106, https://doi.org/10.1594/PANGAEA.899895, 2019.

Grosvenor, D. P., Sourdeval, O., Zuidema, P., Ackerman, A., Alexandrov, M. D., Bennartz, R., Boers, R., Cairns, B., Chiu, J. C., Christensen, M., Deneke, H., Diamond, M., Feingold, G., Fridlind, A., Hünerbein, A., Knist, C., Kollias, P., Marshak, A., McCoy, D., Merk, D., Painemal, D., Rausch, J., Rosenfeld, D., Russchenberg, H., Seifert, P., Sinclair, K., Stier, P., van Diedenhoven, B., Wendisch, M., Werner, F., Wood, R., Zhang, Z., and Quaas, J.: Remote Sensing of Droplet Number Concentration in Warm Clouds: A Review of the Current State of Knowledge and Perspectives, Reviews of Geophysics, 56, 409–453, https://doi.org/10.1029/2017RG000593, 2018.

Hande, L. B., Engler, C., Hoose, C., and Tegen, I.: Parameterizing cloud condensation nuclei concentrations during HOPE, Atmospheric Chemistry and Physics, 16, 12 059–12 079, https://doi.org/10.5194/acp-16-12059-2016, 2016.

Heinze, R., Dipankar, A., Henken, C. C., Moseley, C., Sourdeval, O., Trömel, S., Xie, X., Adamidis, P., Ament, F., Baars, H., Barthlott, C., Behrendt, A., Blahak, U., Bley, S., Brdar, S., Brueck, M., Crewell, S., Deneke, H., Di Girolamo, P., Evaristo, R., Fischer, J., Frank, C., Friederichs, P., Göcke, T., Gorges, K., Hande, L., Hanke, M., Hansen, A., Hege, H. C., Hoose, C., Jahns, T., Kalthoff, N., Klocke, D., Kneifel, S., Knippertz, P., Kuhn, A., van Laar, T., Macke, A., Maurer, V., Mayer, B., Meyer, C. I., Muppa, S. K., Neggers, R. A. J., Orlandi, E., Pantillon, F., Pospichal, B., Röber, N., Scheck, L., Seifert, A., Seifert, P., Senf, F., Siligam, P., Simmer, C., Steinke, S., Stevens, B., Wapler, K., Weniger, M., Wulfmeyer, V., Zängl, G., Zhang, D., and Quaas, J.: Large-eddy simulations over Germany using ICON: a comprehensive evaluation, Quarterly Journal of the Royal Meteorological Society, 143, 69–100, https://doi.org/10.1002/qj.2947, 2017.

Inness, A., Ades, M., Agustí-Panareda, A., Barré, J., Benedictow, A., Blechschmidt, A.-M., Dominguez, J. J., Engelen, R., Eskes, H., Flemming, J., Huijnen, V., Jones, L., Kipling, Z., Massart, S., Parrington, M., Peuch, V.-H., Razinger, M., Remy, S., Schulz, M., and Suttie, M.: The CAMS reanalysis of atmospheric composition, Atmospheric Chemistry and Physics, 19, 3515–3556, https://doi.org/10.5194/acp-19-3515-2019, 2019.

Jäkel, E., Stapf, J., Wendisch, M., Nicolaus, M., Dorn, W., and Rinke, A.: Validation of the sea ice surface albedo scheme of the regional climate model HIRHAM–NAOSIM using aircraft measurements during the ACLOUD/PASCAL campaigns, The Cryosphere, 13, 1695–1708, https://doi.org/10.5194/tc-13-1695-2019, 2019.

Karlsson, J. and Svensson, G.: Consequences of poor representation of Arctic sea-ice albedo and cloud-radiation interactions in the CMIP5 model ensemble, Geophysical Research Letters, 40, 4374–4379, https://doi.org/10.1002/grl.50768, 2013.

Kato, S., Ackerman, T. P., Mather, J. H., and Clothiaux, E. E.: The k-distribution method and correlated-k approximation for a short-wave radiative transfer model, Journal of Quantitative Spectroscopy and Radiative Transfer, 62, 109–121, https://doi.org/10.1016/S0022-4073(98)00075-2, 1999.

Kay, J. E., L'Ecuyer, T., Chepfer, H., Loeb, N., Morrison, A., and Cesana, G.: Recent Advances in Arctic Cloud and Climate Research, Current Climate Change Reports, pp. 1–11, https://doi.org/10.1007/s40641-016-0051-9, 2016.

Klocke, D., Brueck, M., Hohenegger, C., and Stevens, B.: Rediscovery of the doldrums in storm-resolving simulations over the tropical Atlantic, Nature Geoscience, 10, 891–896, https://doi.org/10.1038/s41561-017-0005-4, 2017.

Knudsen, E. M., Heinold, B., Dahlke, S., Bozem, H., Crewell, S., Gorodetskaya, I. V., Heygster, G., Kunkel, D., Maturilli, M., Mech, M., Viceto, C., Rinke, A., Schmithüsen, H., Ehrlich, A., Macke, A., Lüpkes, C., and Wendisch, M.: Meteorological conditions during the ACLOUD/PASCAL field campaign near Svalbard in early summer 2017, Atmospheric Chemistry and Physics, 18, 17 995–18 022, https://doi.org/10.5194/acp-18-17995-2018, 2018.

Knust, R.: Polar Research and Supply Vessel POLARSTERN operated by the Alfred-Wegener-Institute, Journal of large-scale research facilities JLSRF, 3, A119, https://doi.org/10.17815/jlsrf-3-163, http://jlsrf.org/index.php/lsf/article/view/163, 2017.

Korolev, A. and Field, P. R.: The Effect of Dynamics on Mixed-Phase Clouds: Theoretical Considerations, Journal of the Atmospheric Sciences, 65, 66–86, https://doi.org/10.1175/2007JAS2355.1, 2008.

Korolev, A. V., Strapp, J. W., Isaac, G. A., and Nevzorov, A. N.: The Nevzorov Airborne Hot-Wire LWC–TWC Probe: Principle of Operation and Performance Characteristics, Journal of Atmospheric and Oceanic Technology, 15, 1495–1510, https://doi.org/10.1175/1520-0426(1998)015<1495:TNAHWL>2.0.CO;2, 1998.

Kretzschmar, J., Salzmann, M., Mülmenstädt, J., and Quaas, J.: Arctic clouds in ECHAM6 and their sensitivity to cloud microphysics and surface fluxes, Atmospheric Chemistry and Physics, 19, 10 571–10 589, https://doi.org/10.5194/acp-19-10571-2019, 2019.

Levy, R. C., Mattoo, S., Munchak, L. A., Remer, L. A., Sayer, A. M., Patadia, F., and Hsu, N. C.: The Collection 6 MODIS aerosol products over land and ocean, Atmospheric Measurement Techniques, 6, 2989–3034, https://doi.org/10.5194/amt-6-2989-2013, 2013.

Loewe, K., Ekman, A. M. L., Paukert, M., Sedlar, J., Tjernström, M., and Hoose, C.: Modelling micro- and macrophysical contributors to the dissipation of an Arctic mixed-phase cloud during the Arctic Summer Cloud Ocean Study (ASCOS), Atmospheric Chemistry and Physics, 17, 6693–6704, https://doi.org/10.5194/acp-17-6693-2017, 2017.

Lohmann, U., Feichter, J., Chuang, C. C., and Penner, J. E.: Prediction of the number of cloud droplets in the ECHAM GCM, Journal of Geophysical Research: Atmospheres, 104, 9169–9198, https://doi.org/10.1029/1999JD900046, 1999.

Lohmann, U., Quaas, J., Kinne, S., and Feichter, J.: Different Approaches for Constraining Global Climate Models of the Anthropogenic Indirect Aerosol Effect, Bulletin of the American Meteorological Society, 88, 243–250, https://doi.org/10.1175/BAMS-88-2-243, 2007.

Mech, M., Maahn, M., Kneifel, S., Ori, D., Orlandi, E., Kollias, P., Schemann, V., and Crewell, S.: PAMTRA 1.0: the Passive and Active Microwave radiative TRAnsfer tool for simulating radiometer and radar measurements of the cloudy atmosphere, Geoscientific Model Development, 13, 4229–4251, https://doi.org/10.5194/gmd-13-4229-2020, 2020.

Mioche, G., Jourdan, O., Delanoë, J., Gourbeyre, C., Febvre, G., Dupuy, R., Monier, M., Szczap, F., Schwarzenboeck, A., and Gayet, J.-F.: Vertical distribution of microphysical properties of Arctic springtime low-level mixed-phase clouds over the Greenland and Norwegian seas, Atmospheric Chemistry and Physics, 17, 12 845–12 869, https://doi.org/10.5194/acp-17-12845-2017, 2017.

Mironov, D., Ritter, B., Schulz, J.-P., Buchhold, M., Lange, M., and MacHulskaya, E.: Parameterisation of sea and lake ice in numerical weather prediction models of the German Weather Service, Tellus A: Dynamic Meteorology and Oceanography, 64, 17 330, https://doi.org/10.3402/tellusa.v64i0.17330, 2012.

Mlawer, E. J., Taubman, S. J., Brown, P. D., Iacono, M. J., and Clough, S. A.: Radiative transfer for inhomogeneous atmospheres: RRTM, a validated correlated-k model for the longwave, Journal of Geophysical Research: Atmospheres, 102, 16 663–16 682, https://doi.org/10.1029/97JD00237, 1997.

Morrison, H. and Pinto, J. O.: Mesoscale Modeling of Springtime Arctic Mixed-Phase Stratiform Clouds Using a New Two-Moment Bulk Microphysics Scheme, Journal of the Atmospheric Sciences, 62, 3683–3704, https://doi.org/10.1175/JAS3564.1, 2005.

Neggers, R. A. J., Chylik, J., Egerer, U., Griesche, H., Schemann, V., Seifert, P., Siebert, H., and Macke, A.: Local and Remote Controls on Arctic Mixed-Layer Evolution, Journal of Advances in Modeling Earth Systems, 11, 2214–2237, https://doi.org/10.1029/2019MS001671, 2019.

Ovchinnikov, M., Ackerman, A. S., Avramov, A., Cheng, A., Fan, J., Fridlind, A. M., Ghan, S., Harrington, J., Hoose, C., Korolev, A., McFarquhar, G. M., Morrison, H., Paukert, M., Savre, J., Shipway, B. J., Shupe, M. D., Solomon, A., and Sulia, K.: Intercomparison of large-eddy simulations of Arctic mixed-phase clouds: Importance of ice size distribution assumptions, Journal of Advances in Modeling Earth Systems, 6, 223–248, https://doi.org/10.1002/2013MS000282, 2014.

Petty, G. W. and Huang, W.: The Modified Gamma Size Distribution Applied to Inhomogeneous and Nonspherical Particles: Key Relationships and Conversions, Journal of the Atmospheric Sciences, 68, 1460–1473, https://doi.org/10.1175/2011JAS3645.1, 2011.

Phillips, V. T. J., DeMott, P. J., and Andronache, C.: An Empirical Parameterization of Heterogeneous Ice Nucleation for Multiple Chemical Species of Aerosol, Journal of the Atmospheric Sciences, 65, 2757–2783, https://doi.org/10.1175/2007JAS2546.1, 2008.

Pinto, J. O.: Autumnal Mixed-Phase Cloudy Boundary Layers in the Arctic, Journal of the Atmospheric Sciences, 55, 2016–2038, https://doi.org/10.1175/1520-0469(1998)055<2016:AMPCBL>2.0.CO;2, 1998.

Pithan, F. and Mauritsen, T.: Arctic amplification dominated by temperature feedbacks in contemporary climate models, Nature Geoscience, 7, 181–184, https://doi.org/10.1038/ngeo2071, 2014.

Pithan, F., Medeiros, B., and Mauritsen, T.: Mixed-phase clouds cause climate model biases in Arctic wintertime temperature inversions, Climate Dynamics, 43, 289–303, https://doi.org/10.1007/s00382-013-1964-9, 2014.

Possner, A., Ekman, A. M. L., and Lohmann, U.: Cloud response and feedback processes in stratiform mixed-phase clouds perturbed by ship exhaust, Geophysical Research Letters, 44, 1964–1972, https://doi.org/10.1002/2016GL071358, 2017.

Rauber, R. M. and Tokay, A.: An Explanation for the Existence of Supercooled Water at the Top of Cold Clouds, Journal of the Atmospheric Sciences, 48, 1005–1023, https://doi.org/10.1175/1520-0469(1991)048<1005:AEFTEO>2.0.CO;2, 1991.

Ruiz-Donoso, E., Ehrlich, A., Schäfer, M., Jäkel, E., Schemann, V., Crewell, S., Mech, M., Kulla, B. S., Kliesch, L.-L., Neuber, R., and Wendisch, M.: Small-scale structure of thermodynamic phase in Arctic mixed-phase clouds observed by airborne remote sensing during a cold air outbreak and a warm air advection event, Atmospheric Chemistry and Physics, 20, 5487–5511, https://doi.org/10.5194/acp-20-5487-2020, 2020.

Schäfer, M., Loewe, K., Ehrlich, A., Hoose, C., and Wendisch, M.: Simulated and observed horizontal inhomogeneities of optical thickness of Arctic stratus, Atmospheric Chemistry and Physics, 18, 13 115–13 133, https://doi.org/10.5194/acp-18-13115-2018, 2018.

Schemann, V. and Ebell, K.: Simulation of mixed-phase clouds with the ICON large-eddy model in the complex Arctic environment around Ny-Ålesund, Atmospheric Chemistry and Physics, 20, 475–485, https://doi.org/10.5194/acp-20-475-2020, 2020.

Schnaiter, M. and Järvinen, E.: SID-3 1 Hz size distribution of cloud particles during the ACLOUD campaign in 2017, https://doi.org/10.1594/PANGAEA.900261, 2019.

Schnaiter, M., Järvinen, E., Vochezer, P., Abdelmonem, A., Wagner, R., Jourdan, O., Mioche, G., Shcherbakov, V. N., Schmitt, C. G., Tricoli, U., Ulanowski, Z., and Heymsfield, A. J.: Cloud chamber experiments on the origin of ice crystal complexity in cirrus clouds, Atmospheric Chemistry and Physics, 16, 5091–5110, https://doi.org/10.5194/acp-16-5091-2016, 2016.

Schneider, T., Teixeira, J., Bretherton, C. S., Brient, F., Pressel, K. G., Schär, C., and Siebesma, A. P.: Climate goals and computing the future of clouds, Nature Climate Change, 7, 3–5, https://doi.org/10.1038/nclimate3190, 2017.

Screen, J. A. and Simmonds, I.: The central role of diminishing sea ice in recent Arctic temperature amplification., Nature, 464, 1334–1337, https://doi.org/10.1038/nature09051, 2010.

Seifert, A. and Beheng, K. D.: A two-moment cloud microphysics parameterization for mixed-phase clouds. Part 1: Model description, Meteorology and Atmospheric Physics, 92, 45–66, https://doi.org/10.1007/s00703-005-0112-4, 2006.

Serreze, M. C. and Barry, R. G.: Processes and impacts of Arctic amplification: A research synthesis, Global and Planetary Change, 77, 85–96, https://doi.org/10.1016/j.gloplacha.2011.03.004, 2011.

Shupe, M. D. and Intrieri, J. M.: Cloud radiative forcing of the Arctic surface: The influence of cloud properties, surface albedo, and solar zenith angle, Journal of Climate, 17, 616–628, https://doi.org/10.1175/1520-0442(2004)017<0616:CRFOTA>2.0.CO;2, 2004.

Shupe, M. D., Kollias, P., Persson, P. O. G., and McFarquhar, G. M.: Vertical Motions in Arctic Mixed-Phase Stratiform Clouds, Journal of the Atmospheric Sciences, 65, 1304–1322, https://doi.org/10.1175/2007JAS2479.1, 2008.

Solomon, A., Feingold, G., and Shupe, M. D.: The role of ice nuclei recycling in the maintenance of cloud ice in Arctic mixed-phase stratocumulus, Atmospheric Chemistry and Physics, 15, 10 631–10 643, https://doi.org/10.5194/acp-15-10631-2015, 2015.

Solomon, A., de Boer, G., Creamean, J. M., McComiskey, A., Shupe, M. D., Maahn, M., and Cox, C.: The relative impact of cloud condensation nuclei and ice nucleating particle concentrations on phase partitioning in Arctic mixed-phase stratocumulus clouds, Atmospheric Chemistry and Physics, 18, 17 047–17 059, https://doi.org/10.5194/acp-18-17047-2018, 2018.

Sotiropoulou, G., Tjernström, M., Savre, J., Ekman, A. M. L., Hartung, K., and Sedlar, J.: Large-eddy simulation of a warm-air advection episode in the summer Arctic, Quarterly Journal of the Royal Meteorological Society, 144, 2449–2462, https://doi.org/10.1002/qj.3316, 2018.

Stamnes, K., Tsay, S.-C., Wiscombe, W., and Jayaweera, K.: Numerically stable algorithm for discrete-ordinate-method radiative transfer in multiple scattering and emitting layered media, Applied Optics, 27, 2502, https://doi.org/10.1364/ao.27.002502, 1988.

Stapf, J., Ehrlich, A., Jäkel, E., and Wendisch, M.: Aircraft measurements of broadband irradiance during the ACLOUD campaign in 2017, https://doi.org/10.1594/PANGAEA.900442, 2019.

Stapf, J., Ehrlich, A., Jäkel, E., Lüpkes, C., and Wendisch, M.: Reassessment of shortwave surface cloud radiative forcing in the Arctic: consideration of surface-albedo–cloud interactions, Atmospheric Chemistry and Physics, 20, 9895–9914, https://doi.org/10.5194/acp-20-9895-2020, 2020.

Stevens, B., Satoh, M., Auger, L., Biercamp, J., Bretherton, C. S., Chen, X., Düben, P., Judt, F., Khairoutdinov, M., Klocke, D., Kodama, C., Kornblueh, L., Lin, S.-J., Neumann, P., Putman, W. M., Röber, N., Shibuya, R., Vanniere, B., Vidale, P. L., Wedi, N., and Zhou, L.: DYAMOND: the DYnamics of the Atmospheric general circulation Modeled On Non-hydrostatic Domains, Progress in Earth and Planetary Science, 6, 61, https://doi.org/10.1186/s40645-019-0304-z, 2019.

Stevens, B., Acquistapace, C., Hansen, A., Heinze, R., Klinger, C., Klocke, D., Rybka, H., Schubotz, W., Windmiller, J., Adamidis, P., Arka, I., Barlakas, V., Biercamp, J., Brueck, M., Brune, S., Buehler, S. A., Burkhardt, U., Cioni, G., Costa-Surós, M., Crewell, S., Crüger, T., Deneke, H., Friederichs, P., Henken, C. C., Hohenegger, C., Jacob, M., Jakub, F., Kalthoff, N., Köhler, M., van Laar, T. W., Li, P., Löhnert, U., Macke, A., Madenach, N., Mayer, B., Nam, C., Naumann, A. K., Peters, K., Poll, S., Quaas, J., Röber, N., Rochetin, N., Scheck, L., Schemann, V., Schnitt, S., Seifert, A., Senf, F., Shapkalijevski, M., Simmer, C., Singh, S., Sourdeval, O., Spickermann, D., Strandgren, J., Tessiot, O., Vercauteren, N., Vial, J., Voigt, A., and Zängl, G.: The Added Value of Large-Eddy and Storm-Resolving Models for Simulating Clouds and Precipitation, Journal of the Meteorological Society of Japan. Ser. II, https://doi.org/10.2151/jmsj.2020-021, 2020.

Stramler, K., Del Genio, A. D., and Rossow, W. B.: Synoptically driven Arctic winter states, Journal of Climate, 24, 1747–1762, https://doi.org/10.1175/2010JCLI3817.1, 2011.

Tiedtke, M.: A Comprehensive Mass Flux Scheme for Cumulus Parameterization in Large-Scale Models, Monthly Weather Review, 117, 1779–1800, https://doi.org/10.1175/1520-0493(1989)117<1779:ACMFSF>2.0.CO;2, 1989.

Tonttila, J., O'Connor, E. J., Niemelä, S., Räisänen, P., and Järvinen, H.: Cloud base vertical velocity statistics: A comparison between an atmospheric mesoscale model and remote sensing observations, Atmospheric Chemistry and Physics, 11, 9207–9218, https://doi.org/10.5194/acp-11-9207-2011, 2011.

Twomey, S.: The Influence of Pollution on the Shortwave Albedo of Clouds, Journal of the Atmospheric Sciences, 34, 1149–1152, https://doi.org/10.1175/1520-0469(1977)034<1149:TIOPOT>2.0.CO;2, 1977.

Wendisch, M., Brückner, M., Burrows, J., Crewell, S., Dethloff, K., Ebell, K., Lüpkes, C., Macke, A., Notholt, J., Quaas, J., Rinke, A., and Tegen, I.: Understanding Causes and Effects of Rapid Warming in the Arctic, Eos, https://doi.org/10.1029/2017EO064803, 2017.

Wendisch, M., Macke, A., Ehrlich, A., Lüpkes, C., Mech, M., Chechin, D., Dethloff, K., Velasco, C. B., Bozem, H., Brückner, M., Clemen, H.-C., Crewell, S., Donth, T., Dupuy, R., Ebell, K., Egerer, U., Engelmann, R., Engler, C., Eppers, O., Gehrmann, M., Gong, X., Gottschalk, M., Gourbeyre, C., Griesche, H., Hartmann, J., Hartmann, M., Heinold, B., Herber, A., Herrmann, H., Heygster, G., Hoor, P., Jafariserajehlou, S., Jäkel, E., Järvinen, E., Jourdan, O., Kästner, U., Kecorius, S., Knudsen, E. M., Köllner, F., Kretzschmar, J., Lelli, L., Leroy, D., Maturilli, M., Mei, L., Mertes, S., Mioche, G., Neuber, R., Nicolaus, M., Nomokonova, T., Notholt, J., Palm, M., van Pinxteren, M., Quaas, J., Richter, P., Ruiz-Donoso, E., Schäfer, M., Schmieder, K., Schnaiter, M., Schneider, J., Schwarzenböck, A., Seifert, P., Shupe, M. D., Siebert, H., Spreen, G., Stapf, J., Stratmann, F., Vogl, T., Welti, A., Wex, H., Wiedensohler, A., Zanatta, M., and Zeppenfeld, S.: The Arctic Cloud Puzzle: Using ACLOUD/PASCAL Multiplatform Observations to Unravel the Role of Clouds and Aerosol Particles in Arctic Amplification, Bulletin of the American Meteorological Society, 100, 841–871, https://doi.org/10.1175/BAMS-D-18-0072.1, 2019.

Wesche, C., Steinhage, D., and Nixdorf, U.: Polar aircraft Polar 5 and Polar 6 operated by the Alfred Wegener Institute, Journal of large-scale research facilities JLSRF, 2, A87, https://doi.org/10.17815/jlsrf-2-153, 2016.

Zängl, G., Reinert, D., Rípodas, P., and Baldauf, M.: The ICON (ICOsahedral Non-hydrostatic) modelling framework of DWD and MPI-M: Description of the non-hydrostatic dynamical core, Quarterly Journal of the Royal Meteorological Society, 141, 563–579, https://doi.org/10.1002/qj.2378, 2015.